

MICROMECHANICAL ASSESSMENT OF REGIONAL VARIATION IN THE HUMAN LUMBAR INTERLAMELLAR MATRIX

By

Ali Kaissi

*Thesis
Submitted to Flinders University
for the degree of*

Master of Engineering (Biomedical)

College of Science and Engineering
July 11th 2022

Declaration

I hereby acknowledge that in accordance with Flinders University's policies on plagiarism, and unless otherwise referenced, all material presented in this report is my own.

Ali Kaissi

2021/2022

Acknowledgements

I would like to acknowledge the following for their assistance throughout the duration of this project and in the production of this report. The contributions received are greatly appreciated.

- Associate Professor John Costi
- Michael Russo
- Javad Tavakoli
- Atefa Rezwani
- Daniel Kim
- Ushmita Reebye

Table of Contents

Declaration.....	1
Acknowledgements.....	2
Table of Contents.....	3
List of Figures.....	4
List of Tables.....	4
Executive Summary.....	6
1. Introduction.....	6
2. Literature Review.....	8
2.1. Annulus Fibrosus and Interlamellar Matrix Anatomy.....	8
2.2. Mechanical Properties of Lamellae and Interlamellar Matrix.....	10
3. Methodology.....	13
3.1. Specimen Preparation.....	13
3.2. Specimen Mounting.....	17
3.3. Mechanical Testing.....	18
3.4. Data and Statistical Analysis.....	19
3.5. Pilot Testing (Ovine).....	21
4. Results – Data and Statistical Analysis.....	21
4.1. Pilot Tests.....	21
4.2. Primary Results – Human Interlamellar Matrix.....	22
4.2.1. Toe Modulus.....	23
4.2.2. Linear Modulus.....	24
4.2.3. Hysteresis Loss Ratio.....	26
4.2.4. Ultimate Stress and Strain.....	27
5. Discussion.....	30
5.1. Results Interpretation.....	30
5.1.1. Toe Modulus.....	30
5.1.2. Linear Modulus.....	31
5.1.3. Hysteresis Loss.....	33
5.1.4. Ultimate Stress and Strain.....	34
5.2. Limitations of Study.....	35
6. Conclusions.....	36
7. Future Work.....	37
8. References.....	39
Appendix A – Detailed Donor Information and Specimen Dimensions.....	41
Appendix B – Cyclic Loading and Failure Data for All Specimens.....	42

List of Figures

Figure 1: a) Alternating angular orientation and b) crimp angle of collagen fibres in adjacent lamellae	8
Figure 2: Microscopic image depicting the elastic fibre orientation comparison between a) the intra-lamellar matrix and b) the interlamellar matrix (ILM)	9
Figure 3: Cross-bridge structure across multiple lamellae	10
Figure 4: Elastic fibre network and complex ultrastructure of ILM.....	10
Figure 5: Peel test to determine delamination strength	11
Figure 6: Elastic fibre orientation within ILM (a) under tension in and (b) unloaded	12
Figure 7: Sample preparation by Tavakoli (2018) and defined testing directions.	12
Figure 8: Regions of interest within the disc	13
Figure 9: Anterior and lateral view X-ray of L1-L2 from donors D1-D5	14
Figure 10: Isolated discs	15
Figure 11: Microtome slicing process.	16
Figure 12: Smaller segment of AF cut from 2mm thick slice	17
Figure 13: a) depiction of radial tensile and circumferential shear loading directions and the corresponding gripping setup for b) radial tension and c) circumferential shear.	17
Figure 14: a) CellScale BioTester machine with a specimen secured for b) radial tension and c) circumferential shear testing.	18
Figure 15: High resolution images taken during loading of a) radial tension and b) circumferential shear test... 19	19
Figure 16: a) Demonstration of how toe and linear modulus are calculated for each loading curve and b) Hysteresis loss ratio.....	20
Figure 17: Failure curve with ultimate stress and strain at ultimate stress identified.....	20
Figure 18: Pilot test to verify the use of five loading cycles	21
Figure 19: Pilot test to verify the use of five minute rest period duration between tests	22
Figure 20: Example results of stress-strain curves generated from ovine pilot testing for both a) radial tension and b) circumferential shear.	22
Figure 21: Isolated ILM during pilot testing.	22
Figure 22: Example of stress-strain curves from human ILM specimens under a) radial tension and b) circumferential shear.	23
Figure 23: Toe modulus results for slow, medium and fast strain rates grouped by disc region for a) radial tension and b) circumferential shear loading directions.....	23
Figure 24: Linear modulus results for slow, medium and fast strain rates grouped by disc region for a) radial tension and b) circumferential shear loading directions.	24
Figure 25: Hysteresis loss ratio results for slow, medium and fast strain rates grouped by disc region for a) radial tension and b) circumferential shear loading directions.	26
Figure 26: a) Ultimate stress and b) corresponding strain grouped based on disc region for both radial tension and circumferential shear	28
Figure 27: All analysed loading cycles for slow, medium, fast and failure tests for D1.....	42
Figure 28: All analysed loading cycles for slow, medium, fast and failure tests for D2.....	42
Figure 29: All analysed loading cycles for slow, medium, fast and failure tests for D3.....	43
Figure 30: All analysed loading cycles for slow, medium, fast and failure tests for D4.....	43
Figure 31: All analysed loading cycles for slow, medium, fast and failure tests for D5.....	44

List of Tables

Table 1: Summary of ANOVA results for the overall effect on toe modulus of strain rate (slow, medium and fast), and the interactions between strain rate with radial region (outer and inner), circumferential region (anterior and posterolateral) and loading direction (radial tension and circumferential shear)	24
Table 2: Summary of ANOVA results for the overall effect on linear modulus of strain rate (slow, medium and fast), and the interactions between strain rate with radial region (outer and inner), circumferential region (anterior and posterolateral) and loading direction (radial tension and circumferential shear).....	25
Table 3: Bonferroni post-hoc comparison of linear modulus results at slow, medium and fast strain rates, grouped by loading direction and radial region.	25
Table 4: Summary of ANOVA results for the overall effect, on hysteresis loss, of strain rate (slow, medium and fast), and the interactions between strain rate with radial region (outer and inner), circumferential region (anterior and posterolateral) and loading direction (radial tension and circumferential shear).....	27
Table 5: Bonferroni post-hoc comparison of hysteresis loss results at slow, medium and fast strain rates, grouped by loading direction and radial region.	27
Table 6: Summary of results for the overall effect, on ultimate stress, of radial region (outer and inner), circumferential region (anterior and posterolateral) and loading direction (radial tension and circumferential shear), and the interactions between each effect.....	28

Table 7: Effect of loading direction on ultimate stress.....	29
Table 8: Effect of circumferential location on ultimate stress within each radial region and for each loading direction.....	29
Table 9: Summary of results for the overall effect, on ultimate strain, of radial region (outer and inner), circumferential region (anterior and posterolateral) and loading direction (radial tension and circumferential shear), and the interactions between each effect.....	29
Table 10: Effect of loading direction on ultimate strain.....	30
Table 11: Donor age, sex and known relevant health information.....	41
Table 12: Disc dimensions from each specimen, as defined in Table 21, and the approximation of cross-sectional area intact volume.....	41
Table 13: Dimensional symbol definitions of measurements taken from each specimen.....	41

Executive Summary

The lumbar ILM contributes to the overall structural integrity of the intervertebral disc, providing strength and resistance at the boundary between adjacent lamellae, a common site for failure initiation. While there have been previous studies to determine the mechanical properties of the ILM within other species or within human through indirect techniques, the mechanical properties of the human ILM are still predominantly unknown. Gaining a deeper knowledge of the mechanical properties of the human ILM will permit more accurate computational models of the spine in addition to more anatomically accurate future implant design. This study aimed to directly measure the human lumbar ILM micromechanical properties in healthy specimens in both the anatomical radial (tension) and circumferential (shear) loading directions. Regional variations were assessed by obtaining specimens from various circumferential (anterior and posterolateral) and radial (inner and outer) locations within the disc and the viscoelastic behaviour (modulus and energy absorption) assessed by applying the load under three distinct strain rates. The failure mechanics were also investigated through ultimate stress and strain analyses. Extensive pilot testing was conducted on ovine specimens to verify the procedure repeatability prior to the work done on human tissue.

Radial and circumferential regional variations were identified with increased modulus and strength in the outer and anterolateral regions in comparison to inner and posterolateral regions, respectively. Viscoelastic properties of the human ILM were confirmed with a strong strain rate dependence. Furthermore, loading direction had a significant effect on the modulus and ultimate stress, with specimens displaying increased modulus under circumferential shear in comparison to radial tension, and radial tension resulting in a greater ultimate stress. These findings provide a new understanding of the human ILM mechanics as a robust basis for future investigation within the field.

1. Introduction

The human lumbar spine is essential in mobility and functionality, with the intervertebral discs (IVD) acting as the sites of motion for the surrounding musculature to control and manipulate. The annulus fibrosus (AF) forms the surrounding structure of the disc, consisting of adjacent layers of cartilage known as lamellae, provides the majority of the mechanical integrity on a macro scale. The network of fibres and tissue between the lamellae is known as the inter-lamellae matrix (ILM) and the micromechanical properties of which in isolation are still largely uninvestigated with respect to the human spine. Important previous developments have been made in understanding the mechanical properties of the human lumbar AF tissue and single lamellae (Holzapfel, et al. 2005) (Tavakoli, et al. 2016). There have also been steps

taken into further increasing the knowledge of the human ILM micromechanical properties. Previous notable studies include either through indirect methods, such as peel testing (Gregory, et al. 2011) or by making use of other species such as ovine (Tavakoli & Costi, 2018).

These previous studies are yet to isolate a single ILM from a human specimen for mechanical testing purposes and investigate the specific contributions towards the mechanical integrity of the disc provided by the ILM. Furthermore, due to the complex anatomy and geometry resulting in regional variations (Tavakoli, et al. 2016) (Smith & Fazzalari, 2006), mechanical performance differences are expected. Furthering the knowledge of the mechanical properties of the human isolated ILM, with respect to disc region, will provide the ability for more accurate modelling of the human spine, failure modes and longevity predictions through means such as finite element analysis. This research provides new insights useful for the development of spinal implants that better mimic the mechanical and material properties of the human spine.

The aim of this study was to provide new knowledge of the micromechanical properties of the human lumbar ILM with respect to the location within the AF. These micromechanical properties were determined by isolating the lamellae-ILM-lamellae junction of the AF of specimens obtained from human cadavers and conducting various micro-tensile tests in both the radial (tension) and circumferential (shear) directions of the disc. These tests were conducted at various strain rates in order to analyse the viscoelastic properties of the ILM. Samples were taken from radial and circumferential locations throughout the AF to determine the dependence of the mechanical properties on the location within the disc, making distinct comparisons between the outer regions to the inner, transitional region closer to the nucleus. The mechanical properties that were analysed include toe modulus, elastic modulus, ultimate stress and strain, and hysteresis loss ratio (a measure of energy absorption). It is hypothesized that the modulus will be significantly greater for samples obtained from the outer AF when compared to inner AF samples due to the increased elastic fibre density in the outer regions in comparison to the layers closer to the nucleus. Furthermore, the modulus is expected to be lower in posterolateral (rear corner) locations in comparison to the anterior (front) region within the disc due to the weak ILM cohesion within this region. The modulus in the radial direction is also expected to be greater than in the circumferential direction as the ILM purpose is hypothesized as providing mechanical integrity between adjacent lamellae, not in the circumferential direction as the collagen fibres within the lamellae will provide mechanical integrity in this direction.

2. Literature Review

2.1. Annulus Fibrosus and Interlamellar Matrix Anatomy

Human lumbar discs consist of three predominant components; the anulus fibrosus, the nucleus pulposus (NP) and the vertebral end plates (Humzah & Soames, 1988). The superior and inferior end plates of the disc, composed of hyaline cartilage, contain the highly organised and structured annulus fibrosus (AF) which surrounds the less organised, gelatinous NP from lateral, anterior and posterior directions. The anulus fibrosus is composed of concentric cylindrical layers of collagenous tissue known as lamellae (Figure 1), each of which consisting of uniformly arranged collagen fibre bundles (Roberts, et al. 2006).



Figure 1: a) Alternating angular orientation of adjacent lamellae of approximately 30° from vertical axis of the spine (Stewart, et al. 2017) and b) crimp angle and period of collagen fibres in adjacent lamellae illustrated (Gruber & Hanley Jr. 2002).

The human lumbar AF consists of approximately 20-25 distinct lamellae, 0.05-0.5mm in thickness (Newell, et al. 2017) (Inoue & Takeda, 2009), differing dependent upon circumferential location within the disc (Figure 1, red arrows), age and degree of degeneration (Colombini, et al. 2008). The number of distinct layers in the AF is decreased posteriorly in comparison to anterior and lateral locations (Cassidy, et al. 2009) (Marcolongo, et al. 2017), with an increased percentage of incomplete lamellae and looser connection of lamellar bundles in the posterolateral region in comparison to the anterior region (Tsuji, et al. 1993). Furthermore, the number of distinct lamellae is greater for younger discs with lower degrees of degeneration (Marchand & Ahmed, 1990). These lamellae are oriented with the longitudinal axis of the collagen fibres at an average angle of approximately 30° from the vertical axis of the spine (Castro & Lacrois, 2017), with a variation in angle of between 23° and 46° (Holzapfel, et al. 2005). Each lamellae is composed of uniformly oriented collagen fibre bundles with a planar crimped waveform of approximately 20° crimp angle at the periphery of the AF,

increasing to approximately 45° towards the inner AF. Furthermore, the crimp period also decreases from approximately 26µm to 20µm moving from the outer AF to the inner AF (Cassidy, et al. 1989) (Figure 1b). The AF contains both collagen type 1 and type 2, with the ratio of type 1 to type 2 fibres greatest in the outer annulus, decreasing closer to the nucleus of the disc (Bogduk, 1997). In addition to the collagen fibres in the AF, there is also an extracellular matrix of fibres and cells found between the collagen fibres of a single lamellae known as the intra-lamellar matrix (Harvey-Burgess & Gregory, 2019). The outer AF containing ellipsoidal-shaped fibroblast-like cells originating from the mesoderm while the chondrocytes and chondrocyte-like cells of the inner AF originate from the endodermic notochord (Colombini, et al. 2008), providing significant structural distinction with radial region variation (Bruehlmann, et al. 2002). The elastic fibres present in the intra-lamellar matrix have been identified as being oriented parallel to the collagen fibres of the lamellae (Smith & Fazzalari, 2006), providing properties of elasticity to the tissue, allowing recovery after loading (Smith, et al. 2007). These elastic fibres of the intra-lamellar matrix are comprised of hydrophilic elastin surrounded by hydrophilic microfibrils (Colombini, et al. 2008) and are housed within the ground substance, a gelatinous constituent composed of cells within the AF and proteoglycans (PGs) (Buckwalter, 1995). Aggregated PGs consist of a central protein molecule covalently bound to multiple large glycosaminoclycan molecule chains, and ensure that the AF extracellular matrix is hydrated by maintaining hydrostatic pressure (Roughley, 2004) (Colombini, et al. 2008). The molecular size of PGs decreases with age, reducing the discs ability to maintain hydrostatic pressure (Hardingham & Fosang, 1992).

The ILM, with an average thickness of approximately 30µm, consists of elastic fibres that form links between the adjacent lamellae within the AF that resist delamination stresses (Tavakoli, et al. 2017). The orientation of the elastic fibres within the ILM are far less isotropic than found in the intra-lamellar matrix, oriented both parallel and transverse to the collagen fibres (Figure 2) (Smith & Fazzalari, 2006). It has also been identified that there are cross-bridges situated across two or more non-adjacent lamellae, transverse to the longitudinal direction of the collagen fibre network (Tavakoli, et al. 2017). Although the specific origin and contribution of the cross-bridges are unknown,

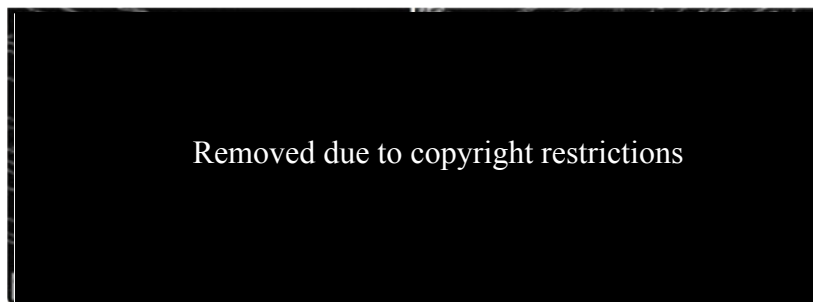


Figure 2: Microscopic image depicting the elastic fibre orientation comparison between a) the intra-lamellar matrix and b) the interlamellar matrix (ILM) (Smith & Fazzalari, 2006).

there is evidence to suggest that they are formed by receded blood vessels during fetal development (Smith & Elliott, 2011). The cross



Figure 3: Cross-bridge structure across multiple lamellae (labelled L5,L7,L9) with the fibrous integration into the collagen network apparent (Schollum, et al. 2008).

bridges have been assessed to find that they form a complex, fine-branching network, with fibres that are deeply integrated with the lamellar structure of the AF (Schollum, et al. 2008) (Figure 3). Similarly to the intra-lamellar matrix, the elastic fibres within the ILM are situated within a proteoglycan-rich ground substance with a heterogeneous density of elastic fibres, both radially and circumferentially (Smith, et al. 2007). Radially, the outer annulus has greater elastic fibre density in comparison to the inner annulus (Tavakoli, et al. 2016) and circumferentially, the posterolateral locations within the disc have a greater density of elastic fibres than the anterolateral locations. The elastic fibre network of the ILM between two adjacent lamellae and the complex interwoven microstructure (Figure 4), as assessed by Tavakoli (2017). This elastic fibre orientation is also non-homogeneous radially within the disc. In the NP and inner AF, a greater proportion of the elastic fibres are oriented radially in comparison to a greater proportion being oriented parallel to the collagen fibre network in the outer AF (Yu, et al. 2002) (Tavakoli, et al. 2016).



Figure 4: Elastic fibre network and complex ultrastructure of ILM (Tavakoli, at al. 2017).


2.2. Mechanical Properties of Lamellae and Interlamellar Matrix

The mechanical properties of the isolated human ILM are still unknown, with previous work focussing on indirect measurement methods or specimens of other species. The mechanical properties of single lamellae collected from the human lumbar AF were studied by Holzapfel, et al. (2005) and Gregory (2012) by means of uniaxial tensile testing. Both studies made use of applying various strain rates to determine the viscoelastic properties of the lamellae tissue collected from outer and inner annulus locations. The study (Gregory, 2012) found that the mean outer elastic modulus was 0.22MPa, having a mean modulus of approximately three times that of the inner samples. Gregory and Callaghan (2011) studied uniaxial and biaxial mechanical properties of the AF in porcine samples to gain a better understanding of more complex stress responses. This study concluded that the AF is under significantly greater stress when subjected to biaxial testing in comparison to uniaxial testing, calculated as 117.9% greater modulus than uniaxial and 82.9% greater modulus than

constrained uniaxial. Further work by Monaco, et al. (2015), provides a comparison between the single lamellar AF tensile properties across various species including ovine, bovine and porcine, allowing a reasonable comparison between results of studies utilising samples from alternate species. The bovine tensile modulus was found to be considerably greater than that of ovine and porcine (1.88MPa, 0.87MPa and 0.47MPa, respectively). Furthermore, these values were all compared to previously found (Holzapfel, et al. 2005) (Gregory & Callaghan. 2012) values of tensile modulus of human AF tensile modulus of 0.22MPa. The effect of various types of loading and mechanical stresses on the mechanical properties and structure of the human AF has also been investigated. In 2018, Harvey-Burgess and Gregory determined the effect of axial torsion and compression on the mechanical properties of the human AF. It was discovered that the mechanical strength of the ILM was not impacted by axial torsion or compression, however the intra-lamellar matrix strength of samples exposed to axial torsion was found to be decreased by 48% in comparison to those not exposed to torsion. The impact of vibration on the intra-lamellar strength was also investigated (Gregory & Callaghan, 2011) by conducting uniaxial tensile testing in the direction perpendicular to the longitudinal orientation of the collagen fibres. It was determined that the vibrated tissue resulted in an increased toe region (stretch ratio of 1.50 compared to 1.31 in non-vibrated samples), hypothesized as being due to damaged elastin.

The mechanical properties of the AF ILM have been investigated in the past through various methodologies, in alternate species or indirect measurement methods. Gregory, et al. (2011) conducted an investigation into the delamination strength of the human AF by peeling apart adjacent lamellae during a peel test, to indirectly measure the strength of the ILM (Figure 5). This testing was conducted on specimens obtained from outer and inner AF locations, anterior and posterior location, and at two different strain rates. The average peel strength was found to be approximately 0.5MPa with approximately 33% increased strength in superficial samples compared to deep and no significant difference between posterior and anterior locations.

Furthermore, the strain rate also did not have a significant impact on the peel strength of the samples. This methodology gives a valuable base understanding for the ILM strength but can be improved to gain results more specific ILM mechanical properties in isolation. Smith, at al. (2007) also measured the tensile mechanical properties of the AF across multiple lamellae in the radial direction, determining the strength of the ILM without isolating a single lamellae-ILM-lamellae junction. This tensile testing was done after enzymatic digestion processes to



Removed due to
copyright
restrictions

Figure 5: Peel test to determine delamination strength (Gregory, et al. 2011).

isolate the elastic fibres and determine their specific contribution. A histological assessment during this study determined that while undergoing radial tension, the orientation of the elastic fibres was perpendicular to the longitudinal direction of the collagen fibres (Figure 6), indicating that the elastic fibres under tension were that of the ILM linking adjacent lamellae. It was determined that the initial and ultimate modulus significantly decreased in the absence of elastic fibres, while the extensibility significantly increased.

Removed due to copyright restrictions

Figure 6: Elastic fibre orientation variation within ILM (a) under radial tension in comparison to (b) unloaded (Smith, et al. 2007).

Tavakoli and Costi (2018) delivered important developments in ILM mechanical testing with ovine specimens, providing essential base knowledge for methodologies that can be applied to the human ILM. The ILM was isolated and tested in circumferential and radial direction (Figure 7) at three different strain rates. Viscoelastic properties of the ILM were confirmed in this study by showing significant strain-rate dependence. Furthermore, the modulus and failure stress was found to be significantly greater in the radial direction in comparison to the circumferential direction. In particular, this work has provided a thorough understanding and repeatable methodology that can be applied to human ILM.

Removed due to copyright restrictions

Figure 7: (a)-(c) Sample preparation by Tavakoli (2018) and (d)-(g) defined testing directions.

A recent investigation by Kandil, et al. (2020) to utilise bovine data to estimate human disc mechanics determined an increased stiffness in the outer AF region in comparison to inner regions due to the increased collagen fibre content. Furthermore, the stiffness in the posterolateral region was identified as being significantly lesser than in the anterior region as

predicted by the increased collagen fibre orientation angle difference (Noailly, et al. 2010). It has also been identified that the angle difference between collagen fibre orientation is greater in the outer AF in comparison to the inner AF, leading to potential contributions to regional mechanical responses (Pezowicz, 2010) (Noailly, et al. 2010). A greater knowledge of the regional variation in mechanical properties of the ILM will also provide a greater context for the reasons behind the lumbar posterolateral region being the most common site for disc failure and herniation (Wathen, et al. 2018) (Donegan & Chin, 2009). While studies have attempted to better understand the ILM, anatomical variations make it challenging to determine the mechanical properties (i.e. regional variation). Therefore, it is important to build on the knowledge from previous studies and to measure the mechanical properties of the human ILM directly while considering regional variations. This study aimed to address this gap in the current literature by directly measuring the human ILM mechanical properties with respect to circumferential and radial regions within the disc.

3. Methodology

All presented methods were validated in an ovine model to ensure repeatability and meticulousness when testing on a human model. After preparation, each specimen is loaded either under radial tension or circumferential shear with a focus on the effect of various loading directions in addition to regional variation (Figure 8) and strain rate.

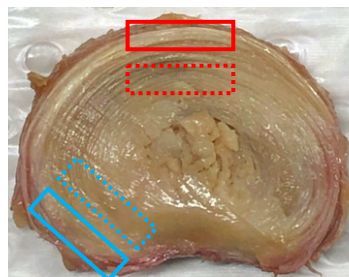


Figure 8: Regions of interest within the disc that were assessed (Red = anterior, blue = posterolateral, solid line = outer, dashed line = inner).

3.1. Specimen Preparation

Pilot data (Section 3.5) was inputted into A Priori power analysis (G*Power Version 3.1.9.6, Heinrich Heine University, Dusseldorf) and it was determined that a minimum of N=5 specimens was required to detect a large effect size of 0.8 standard deviations for this study (Cohen's Criteria). In order to conduct this study, human donor spines of minimal degeneration were obtained (United Tissue Network, USA). Donors were screened for relevant health information (i.e. scoliosis, osteoporosis, smoking, degenerative diseases, etc.) and selected donors were allocated a donor ID from D1-D5 (Appendix A).

Each spinal column was X-Ray imaged, from anterior and posterolateral positions (Figure 9), prior to isolating the disc and testing. These images were used to determine the approximate

volume of the lumbar discs and to identify the relative degenerative state based on disc height. From the imaging and to best mitigate the effects of degeneration on the results, L1-L2 discs were focused on for this study.

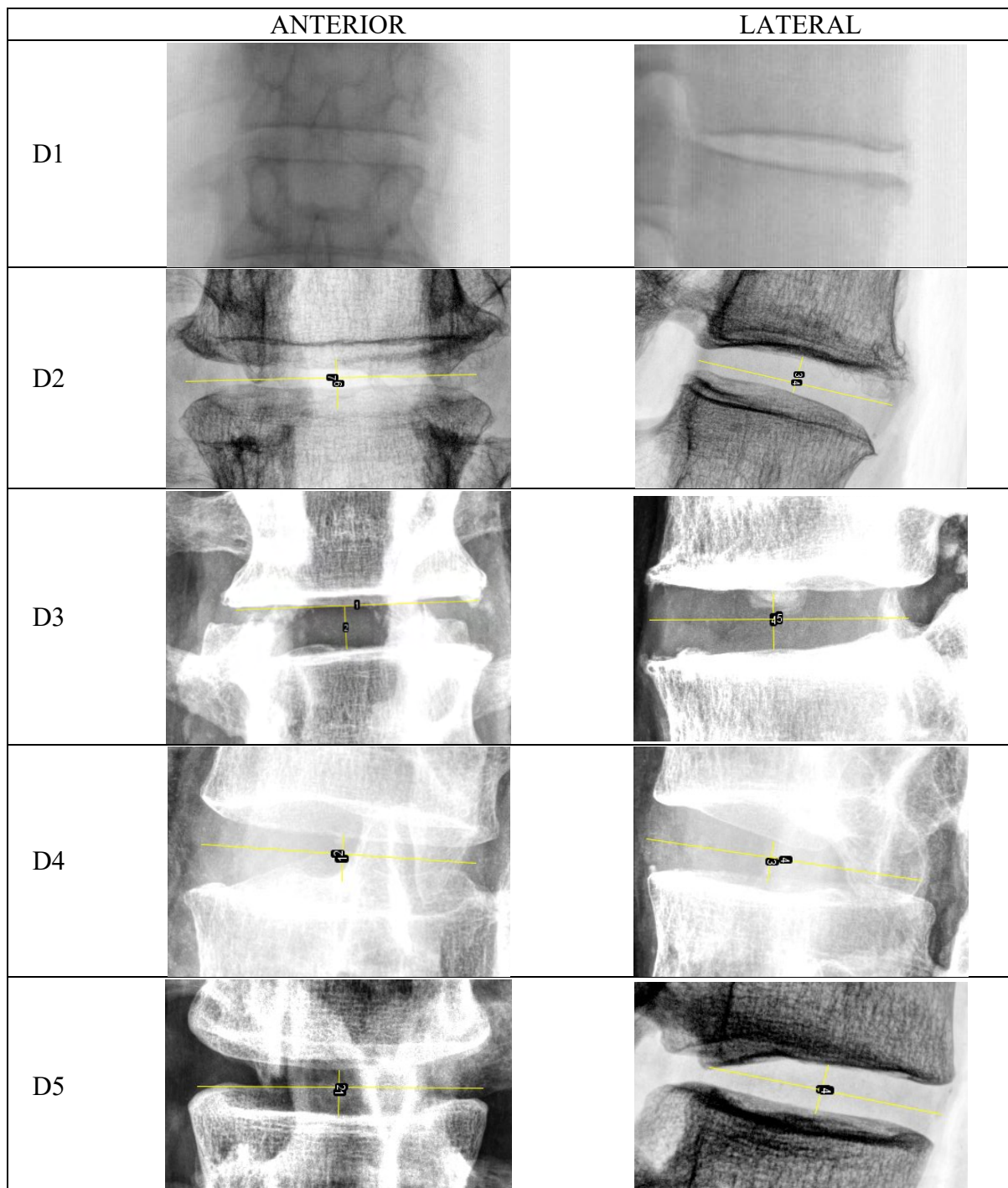


Figure 9: Anterior and lateral view X-ray of L1-L2 from donors D1-D5 with width, height and depth indicated.

The approximate dimensions of the L1-L2 discs of interest were measured using ImageJ 1.8.0 (National Institute of Health, Bethesda, MD, USA). The dimensions taken were disc height, being the distance between adjacent end-plates, the width, being the most lateral distance across the disc and the depth, being the distance from the anterior edge to the posterior edge of the disc. The measurements were taken while the functional spinal unit (FSU) was still

intact to mitigate any disruptive effects that dissection may have on the dimensions of the disc and to provide bony landmarks for assessment. These dimensions were then used to make a volumetric approximation of each disc by using an average between the heights measured from the anterior and lateral view, H_A and H_L respectively, in conjunction with an average between the width (W) and depth (D) for the diameter and a coefficient of 0.84 (equation (i)) (Nachemson & Morris, 1964).

$$V = 0.84\pi \left(\frac{W+D}{4}\right)^2 \left(\frac{H_A+H_L}{2}\right) \quad (i)$$

From these dimensional measurements and volume approximations (Appendix A), the average height was measured as $10.9 \pm 0.47\text{mm}$ with an average approximated volume of $29726 \pm 2618\text{mm}^3$ ($\mu \pm \sigma_M$).

The L1-L2 disc was dissected from the spinal column of each donor (Figure 10), using a hand-mounted blade. Once isolated, each disc was then sprayed with phosphate buffered saline (PBS) solution, individually wrapped in paper and cling wrap and stored in the freezer at approximately -20°C until removed for further specimen preparation. The 7.4pH PBS solution, containing AR grade sodium chloride, potassium chloride, phosphates and distilled water, is used to mitigate the dehydration of the disc by maintaining anatomical hydrostatic pressure (Martin, et al. 2006), where the use of water could result in tissue damage.

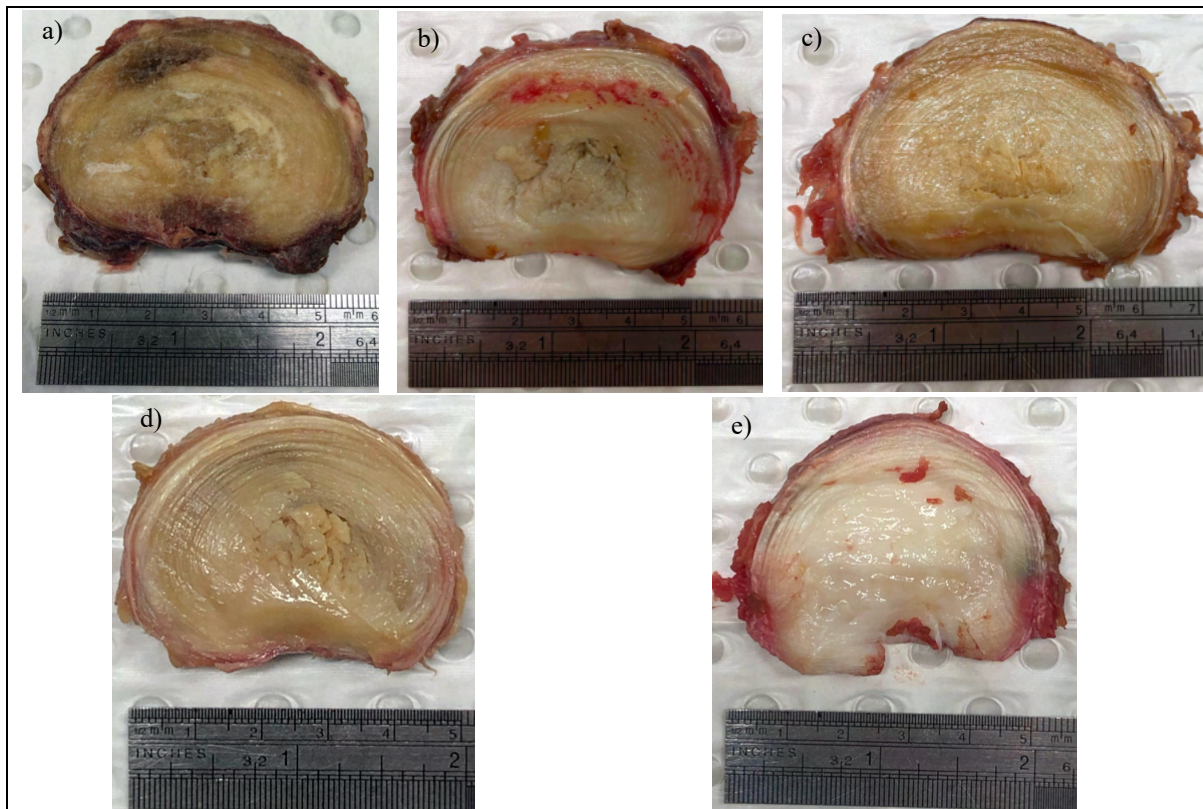


Figure 10: Isolated discs with any visible discoloration due to the presence of blood-containing tissue or end-plate cartilage. [a, b, c, d, e] = [D1, D2, D3, D4, D5], respectively.

Segments from regions of interest (ROI), the anterior and posterolateral regions, were then isolated from the rest of disc (Figure 11a) using a scalpel blade. All cuts through the tissue were made while the disc was still in a frozen state as it was found to allow for a more precise incision. A hand microtome (Figure 11b) and optimal cutting temperature compound (OCT, Tissue-Tek, Sakura, Japan) were used to make transverse slices through the segment of uniform thickness. The OCT allows the specimen to be frozen into a mass of specified shape, allowing for easier slicing of the tissue. A 3D part was designed using Inventor (Autodesk, San Rafael, CA, USA) and printed using Ultimaker 2+ (Ultimaker BV, Utrecht, Netherlands) as a platform to place the specimen on during transverse cutting (white component, Figure 11c). A small channel, concentric to the platform, was added for the OCT to flow into and fix to, restricting the specimen from sliding during cutting. Initially, a thin layer of OCT is spread on the platform, before being placed in the freezer at -20°C for 15 minutes to solidify, in order to ensure that the specimen is not in direct contact with the platform. The specimen is then placed on top of the stage and covered with additional OCT until completely submerged (Figure 11d), and placed again in the freezer for 25 minutes to solidify. PVC tape was used as a boundary around the platform to allow the OCT to freeze in a cylindrical shape for slicing (Figure 11e-f). Once solid, the tape is removed, the platform is lowered on the microtome until only a thin portion of the specimen is raised from the microtome surface. This portion is then sliced using the blade to create a flat superior surface before the microtome is raised in 2mm increments for each following slice (Figure 11g). The microtome has a resolution of 0.01mm to which it can be raised/lowered based on the rotating scale on the device.

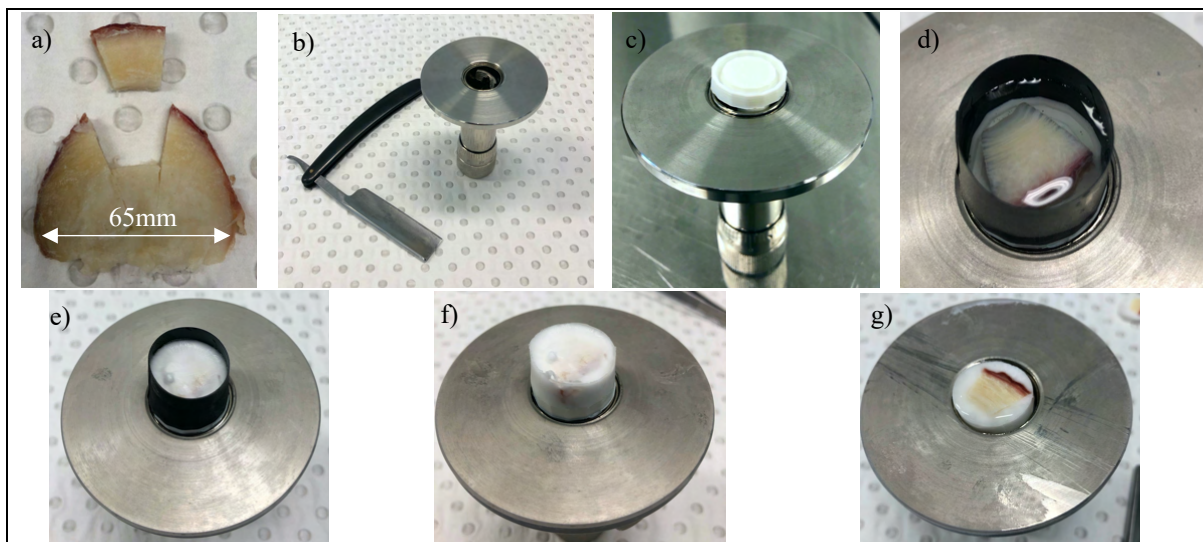


Figure 11: Microtome slicing process. a) hand microtome and blade used, b) microtome with 3D-printed part in place, c) anterior region separated from the disc, d) specimen submerged in OCT compound, e) specimen frozen in OCT compound before and f) after the tape is removed, g) specimen after transverse slice has been made.

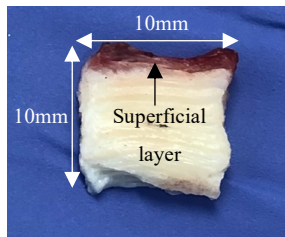


Figure 12: Smaller segment of AF cut from 2mm thick slice with approximate dimensions.

Once the 2mm thick slices of AF have been made, these slices were then cut into specimens of smaller areas from the inner and outer AF of the anterior and posterolateral regions prepared (Figure 12) in preparation for mechanical testing. In the context of this study, the outer AF is defined as between 1-5 distinct lamellae from the superficial layer and the inner AF is defined as between 10-15 distinct lamellae from the superficial layer by identifying the visible structural variation under an illuminated magnifying lens.

3.2. Specimen Mounting

After specimens were sectioned and shaped, they are secured to sandpaper (400 grit) with cyanoacrylate adhesive in one of two ways dependent on the loading direction used for the specific specimen. Four segments of sandpaper are secured to two adjacent lamellae on both the top and underside, leaving the isolated ILM junction unsecured as the subject of the mechanical tests. The two loading directions investigated in this study are in the radial tension and circumferential shear directions, with the load being applied normal to the lamellae orientation for the radial tension setup and the load being applied parallel to the lamellae orientation for the circumferential shear setup (Figure 13a).

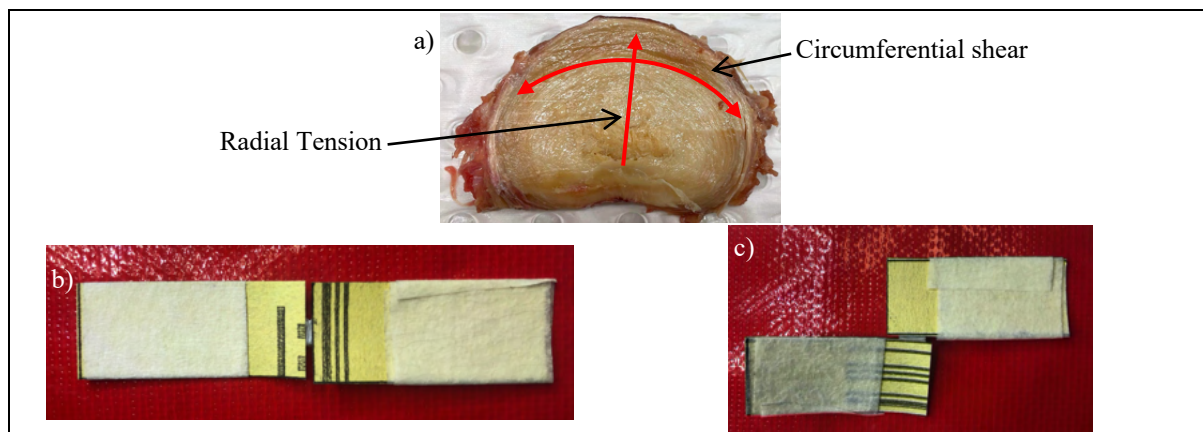


Figure 13: a) depiction of radial tensile and circumferential shear loading directions that will be investigated and the corresponding gripping setup for b) radial tension and c) circumferential shear.

Measurements of the region of interest exposed between the sandpaper grippers were made using digital callipers of resolution 0.01mm to input as the initial dimensions for testing. The BioTester 3000 (CellScale Biomechanics Testing, Waterloo, ON, Canada) load cell was zeroed and then the specimen was fixed to the linear actuator arms with screwing clamps (Figure 14). The specimens were left secured in the BioTester while submerged in a PBS solution bath under nominal load for ten minutes at an anatomical 37°C to allow for hydrostatic equilibrium to be reached before mechanical testing is commenced, and remain submerged at this temperature during testing.

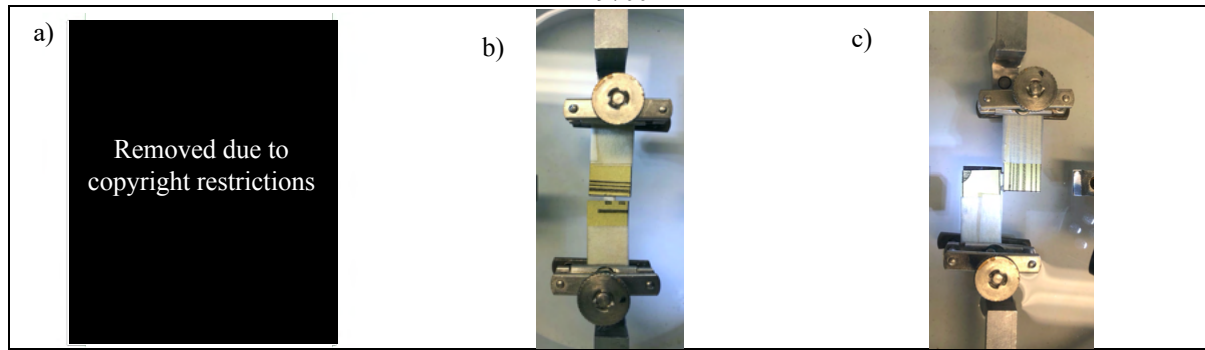


Figure 14: a) CellScale BioTester machine with a specimen secured for b) radial tension and c) circumferential shear testing.

3.3. Mechanical Testing

A uniaxial displacement-control tensile testing protocol was followed for each specimen through the manipulation of the BioTester's end effectors, attached to a 23N load cell using LabJoy (CellScale Biomaterials Testing, Waterloo, ON, Canada) software. A non-destructive 40% strain was applied to each specimen, based on the initial dimensions, to ensure the specimens were loaded in their elastic region (Tavakoli, 2018). Five triangular waveform loading cycles were performed to enable the tissue to reach its steady state under dynamic loading conditions. A pilot test (section 3.5) was conducted to confirm that five loading cycles is ideal to overcome any tissue reorganisation contributions to the mechanical test results. The set of five loading cycles were applied, in the order presented, at three strain rates, $0.1\%s^{-1}$ (slow), $1\%s^{-1}$ (medium) and $10\%s^{-1}$ (fast), with a five minute unloaded rest period between each strain-rate. A preload of 100mN was applied directly prior to the first cycle of each loading block.

The rest period and preload are implemented to minimise creep between tests (Tavakoli, 2018), with the rest period being verified by a pilot test on ovine tissue (see section 3.5). After the final fast strain-rate loading is complete, another five minute rest period was conducted. Following this, a ramp test to failure at the fast strain rate was conducted to assess the failure mechanics of the specimen. Each of these loading groupings, including the failure test, were compiled into a single batch protocol to allow the entire testing protocol for each specimen to run without any human manipulation or intervention required.

An integrated high-resolution imaging system is used to assess the specimens throughout the testing period by taking images (i.e. Figure 15) at a frequency set to 15Hz. Incidence of slippage was monitored by the visibility of relative movement between the gripper edge and the specimen, indicating an insecure fixation. The identification of any slippage at the specimen-gripper interface or premature failure resulted in the data being discarded and a new specimen being prepared for testing.

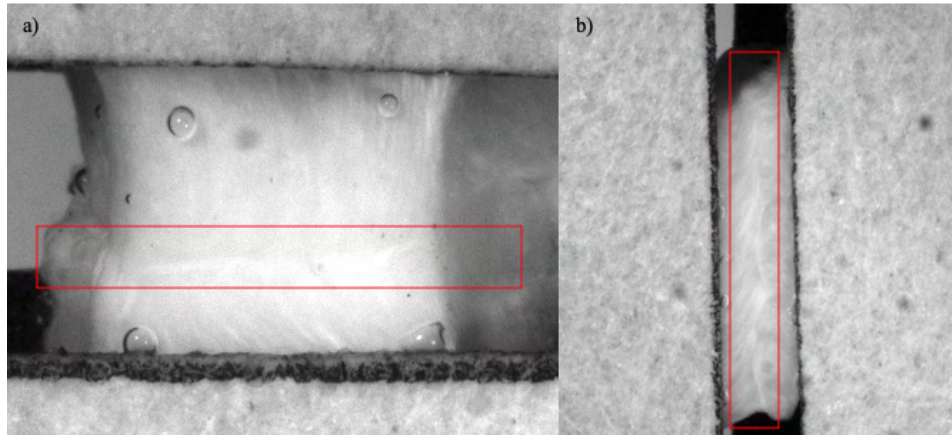


Figure 15: High resolution images taken during loading of a) radial tension test and b) circumferential shear test highlighting the isolation of a single ILM (red box).

3.4. Data and Statistical Analysis

The results from each data set are recorded as values of force as a function of displacement, for which all the data is converted to a stress-strain relationship and analysed using custom written programs using MATLAB R2021b (Mathworks, Natick, MA, USA) software. The force experienced by the specimen is converted to stress by the use of equation (ii).

$$\sigma = \frac{F}{A} \quad (\text{ii})$$

Where σ represents stress, analysed in units of kPa for this study, F represents the force measured and A represents the area over which the force is applied, as calculated from the initial dimensions of the specimen at nominal load in the BioTester. The strain applied to the specimen is calculated from the displacement by the use of equation (iii).

$$\varepsilon = \frac{\Delta L}{L_0} \quad (\text{iii})$$

Where ε represents the strain applied, analysed in units of % for this study, ΔL represents the change in length (displacement) along the axis on which the load is applied and L_0 represents the initial length of the specimen along the loading axis.

Each specimen's stress-strain curve from the final loading cycle for the slow, medium and fast strain rate tests was analysed (Appendix B), calculating the toe modulus, the linear modulus and the hysteresis loss ratio. The toe modulus and linear modulus are calculated as the gradient of the loading portion of the stress-strain curve within the toe region and the linear region, respectively. The toe region and linear region are identified by individually assessing the curve from each specimen and identifying a point of inflection (POI) at which there is a visible change in the slope. Toe modulus is calculated between 0% strain and 10% before the identified POI and the 10% strain following the POI is the region which the linear modulus is calculated (Figure 16a). The hysteresis loss ratio is also calculated to determine the energy absorption of the specimen during the final loading cycle. Hysteresis loss ratio is calculated as the area within the loading-unloading curve divided by the total area under the loading curve

(Figure 16b). The hysteresis loss ratio is assessed rather than the hysteresis area due to the value being normalized by the absolute stress values, allowing for a directly comparable value between specimens.

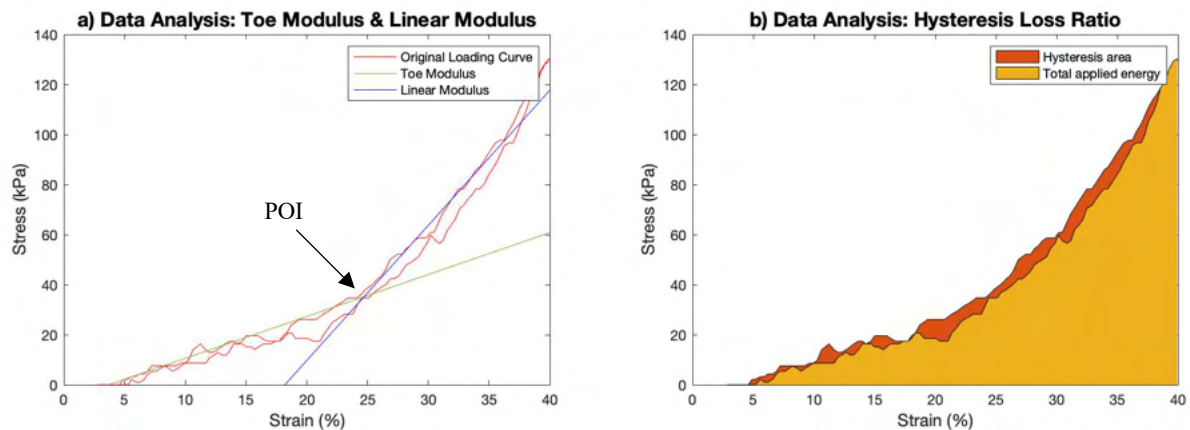


Figure 16: a) Demonstration of how toe and linear modulus are calculated for each loading curve and b) Hysteresis loss ratio calculated as the hysteresis area (orange) divided by the total energy applied to the specimen (orange + yellow).

The failure curve of each specimen is also analysed to obtain the ultimate stress and the strain at which this ultimate stress is occurring. The ultimate stress is found as the maximum stress experienced by the specimen during the failure test and the strain at which this ultimate stress is reached (Figure 17).

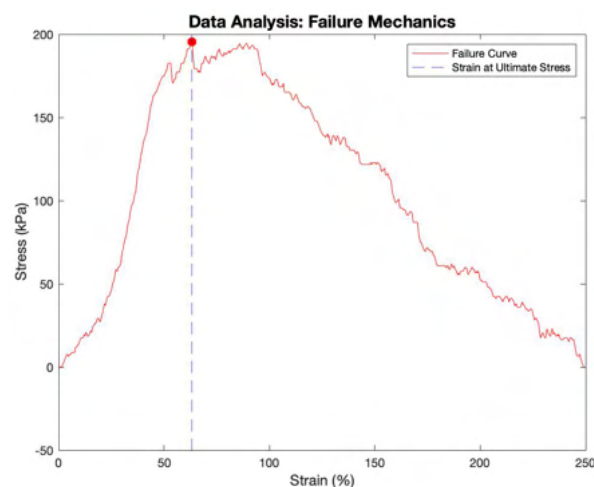


Figure 17: Failure curve with ultimate stress and strain at ultimate stress identified.

A statistical analysis was then conducted on the results for toe modulus, linear modulus, hysteresis loss ratio, ultimate stress and ultimate strain to determine the statistical significance of any trends. Since each specimen underwent loading at three strain rates, separate repeated measures ANOVA tests were conducted (IBM SPSS Statistics for Mac, version 28.0.1.1, IBM Corp., Armonk, NY, USA), while a univariate general linear model is used to determine the effects direction on the ultimate stress and ultimate stress strain results. Each of these statistical tests used a significance threshold, alpha of 0.05 with overall effects and interaction effects analysed. Where significance is identified, Bonferroni post-hoc comparisons were conducted

to determined specific test comparisons for significance. For further analysis purposes, a significance of $0.05 < p < 0.1$ will be identified as marginally significant.

3.5. Pilot Testing (Ovine)

Pilot testing was conducted on ovine specimens prior to commencing investigation on human tissue. Although variations have been reported (Monaco, et al. 2015), ovine discs are widely accepted as a suitable surrogate for human tissue in spine biomechanics. Multiple specimens from a sample size of approximately ten ovine discs, were tested in order to satisfy a repeatable methodology before moving to human specimens. It was vital to reach a high standard of repeatability with the method before the human testing. The aspect of this experimental procedure requiring the greatest preparation through repetition was securing the sandpaper grippers to the adjacent lamellae of the specimen ensuring that one singular ILM is exposed for mechanical testing. Pilot tests were also conducted for the purpose of rest period duration and loading cycle iterations. In order to assess the loading cycle iterations, three ovine specimens were loaded and the relative force experienced by the specimens during each cycle was considered. In order to verify the chosen rest period between tests, a sample size of three ovine specimens was tested at a fast strain rate for five loading cycles, then unloaded (rest period) for five minutes, before undergoing the same cyclic loading for another five cycles. An assumption was made during this pilot test that the time sufficient for the specimen to recover after being loaded at a fast strain rate would also be sufficient at subsequently slower strain rates. The fast strain rate will cause the greatest frictional drag forces within the tissue as fluid flows due to loading, resulting in the greatest ILM stresses requiring recovery in comparison to medium and slow strain rates.

4. Results – Data and Statistical Analysis

4.1. Pilot Tests

Throughout pilot testing, approximately 10 ovine discs were tested in order to verify the experimental procedure prior to commencing testing on human specimens. From investigating the loading cycle iterations, it was found that throughout the first three cycles of the test, the force experienced continued to significantly decrease in maximum amplitude in comparison to the previous cycle, while the variance reduced for cycles four and five. This indicates that the

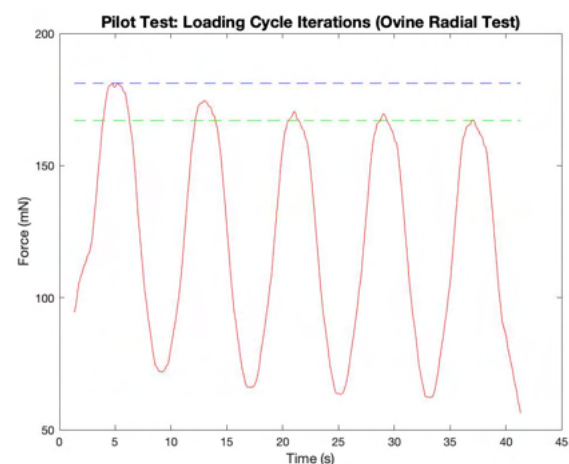


Figure 18: Pilot test to verify the use of five loading cycles, with the dashed lines demonstrating the variation between the first and fifth loading cycle.

reorganisation of the tissue is occurring and takes 3-5 cycles before the majority of reorganisation has occurred at a fast strain rate, (Figure 18). From the rest period validation tests, the force results from the fifth cycle of the second set of dynamic loading was compared with the fifth cycle of the first set and found to have minimal variation (Figure 19), indicating that five minutes of rest is sufficient to allow the specimen to recover between tests.

Figure 19: Pilot test to verify the use of five minute rest period duration between tests, indicated by the similarity in performance of the final cycle of each set

In addition to the rest period and cycle iteration verification, the viscoelastic behaviour of the ovine specimens was assessed to validate the procedure against previous research (Tavakoli & Costi, 2017). The slow strain rate was not tested for the majority of specimens in the interest of time restrictions, with the fast and medium cycles (Figure 20) being analysed. The ability to isolate the ILM was verified (Figure 21) using the high-resolution camera on the BioTester. Furthermore, the gripping methods were verified during pilot testing by ensuring that no slippage occurred during loading, demonstrating that the fixation was secure.

Figure 20: Example results of stress-strain curves generated from ovine pilot testing for both a) radial tension and b) circumferential shear.



Figure 21: Isolated ILM (dashed line) during pilot testing.

4.2. Primary Results – Human Interlamellar Matrix

Stress-strain curves produced for each human specimen per region were used for analysis for both radial tension and circumferential shear on the human specimens (Figure 22).

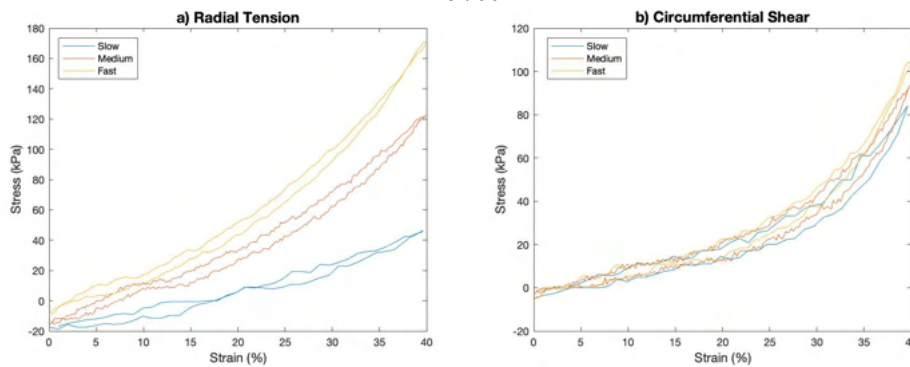


Figure 22: Example of stress-strain curves from human ILM specimens under a) radial tension and b) circumferential shear.

4.2.1. Toe Modulus

The toe modulus within each disc region, for both radial tension and circumferential shear, was grouped by strain rate (Figure 23), with the effect of loading directions, strain rate and disc region assessed.

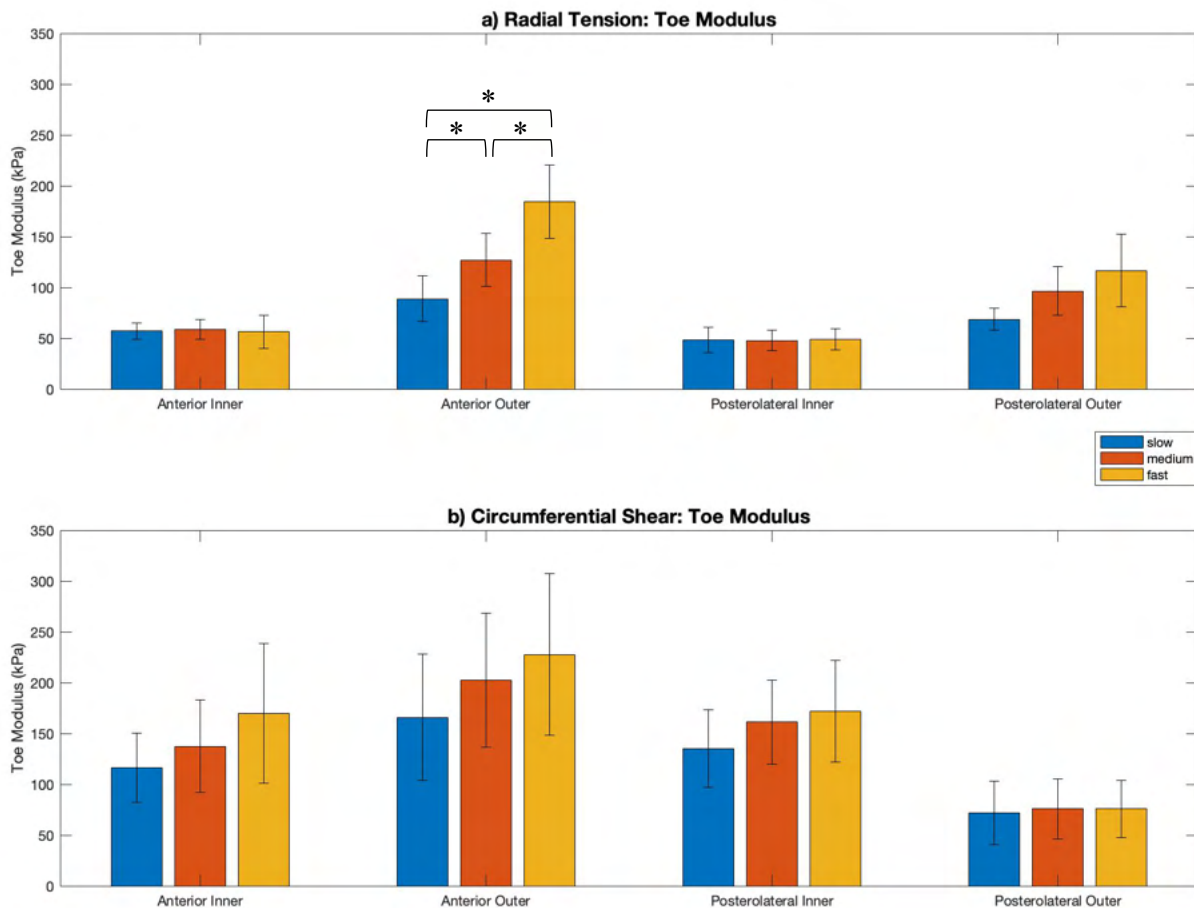


Figure 23: Toe modulus mean with standard error bars for slow, medium and fast strain rates grouped by disc region for a) radial tension and b) circumferential shear loading directions. (* indicates statistically significant difference between results).

The overall effect of strain rate (slow, medium, fast) on the toe modulus result was significant ($p=0.002$) with the interactions between strain rate and the tested independent variables demonstrating non-significant effects (Table 1). Due to the data being not normally distributed, as determined by Mauchly’s test of sphericity, the Greenhouse-Geisser method was used to assess the repeated measures ANOVA results. Strain rate had a highly significant effect

on the toe modulus results with an increased strain rate resulting in a greater modulus. The distinction between strain rate results was much more evident in the outer disc regions in comparison to the inner, particularly under radial tension. The subsequent interactions provided no further significant effects, therefore a post-hoc analysis was not conducted.

Table 1: Summary of ANOVA results for the overall effect on toe modulus of strain rate (slow, medium and fast), and the interactions between strain rate with radial region (outer and inner), circumferential region (anterior and posterolateral) and loading direction (radial tension and circumferential shear). Red and * symbol denoting statistical significance as defined by chosen alpha value (0.05), and yellow representing marginal significance ($0.05 < p < 0.1$).

Statistical Significance of Variable Effects on Toe Modulus	
Interaction	Significance (p-value)
Strain Rate	0.002*
Strain Rate * Radial Region	0.213
Strain Rate * Circumferential Region	0.195
Strain Rate * Loading Direction	0.876
Strain Rate * Radial Region * Circumferential Region	0.350
Strain Rate * Radial Region * Loading Direction	0.070
Strain Rate * Circumferential Region * Loading Direction	0.807
Strain Rate * Radial Region * Circumferential Region * Loading Direction	0.717

4.2.2. Linear Modulus

The linear modulus of each specimen within the linear region was also assessed for each region of interest under both tensile and shearing loading conditions (Figure 24).

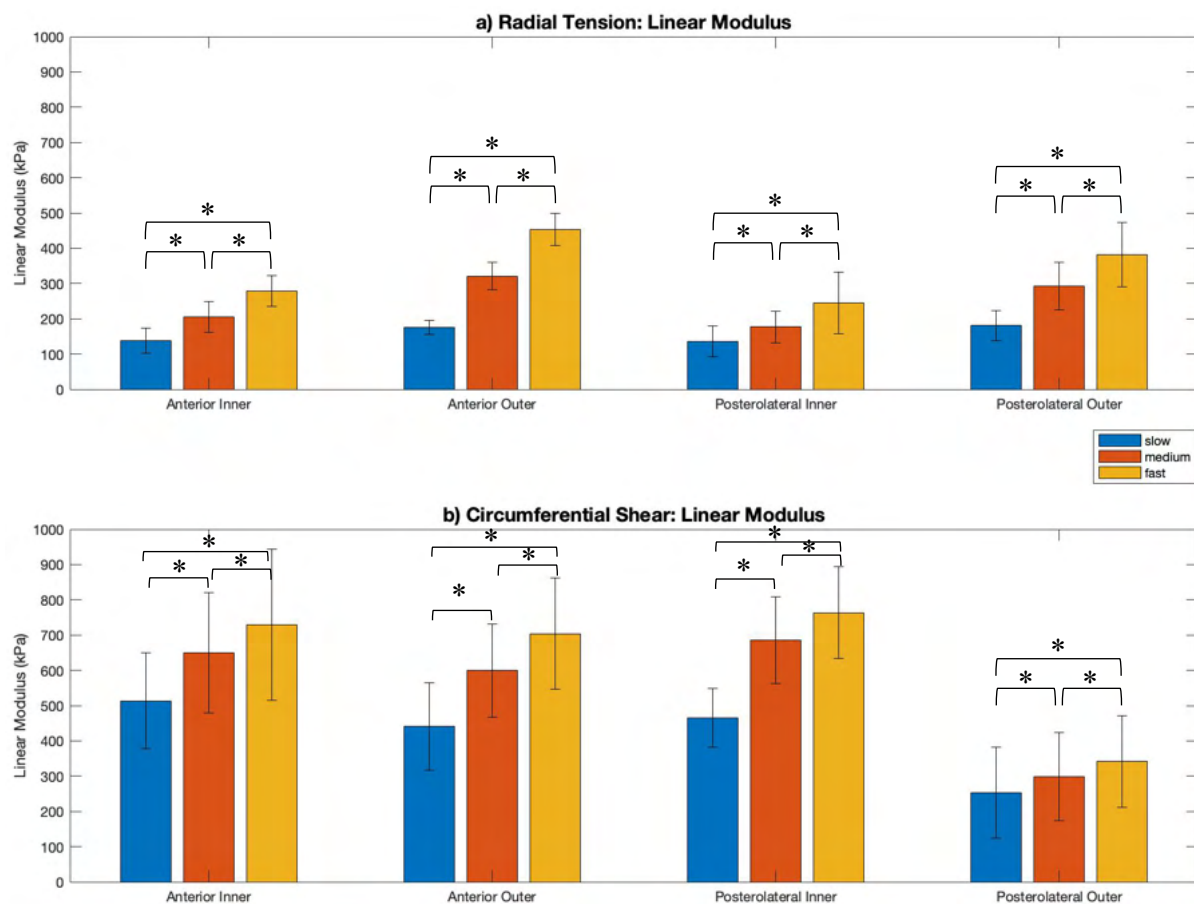


Figure 24: Linear modulus mean with standard error bars for slow, medium and fast strain rates grouped by disc region for a) radial tension and b) circumferential shear loading directions. (* indicates statistically significant difference between results).

The overall effect of strain rate (slow, medium, fast) on the linear modulus result was significant ($p < 0.001$). From the further interactions between strain rate and the other tested variables, a significant effect ($p = 0.014$) was also determined for the interaction between strain rate, radial region and loading direction (Table 2). Due to the data being not normally distributed, as determined by Mauchly's test of sphericity, the Greenhouse-Geisser method was used to assess the repeated measures ANOVA results. Strain rate had a highly significant effect on the linear modulus results with an increased strain rate resulting in a greater modulus. Furthermore, the ILM demonstrated greater linear modulus when loaded under circumferential shear in comparison to radial tension.

Table 2: Summary of ANOVA results for the overall effect on linear modulus of strain rate (slow, medium and fast), and the interactions between strain rate with radial region (outer and inner), circumferential region (anterior and posterolateral) and loading direction (radial tension and circumferential shear). Red and * symbol denoting statistical significance as defined by chosen alpha value (0.05), and yellow representing marginal significance ($0.05 < p < 0.1$).

Statistical Significance of Variable Effects on Linear Modulus	
Interaction	Significance (p-value)
Strain Rate	<0.001*
Strain Rate * Radial Region	0.701
Strain Rate * Circumferential Region	0.244
Strain Rate * Loading Direction	0.246
Strain Rate * Radial Region * Circumferential Region	0.067
Strain Rate * Radial Region * Loading Direction	0.014
Strain Rate * Circumferential Region * Loading Direction	0.899
Strain Rate * Radial Region * Circumferential Region * Loading Direction	0.169

A Bonferroni post-hoc analysis determined that there is a significant effect ($p < 0.001$) of strain rate between each test grouped by radial region and loading direction, irrespective of circumferential region (Table 3). The circumferential region is not considered in this post-hoc comparison due to providing no overall significant effects on linear modulus.

Table 3: Bonferroni post-hoc comparison of linear modulus results at slow, medium and fast strain rates, grouped by loading direction and radial region. Red and * symbol denoting statistical significance as defined by chosen alpha value (0.05), and yellow representing marginal significance ($0.05 < p < 0.1$).

Bonferroni Post-hoc Analysis of Linear Modulus Comparisons				
Loading Direction	Radial Region	Linear Modulus (1)	Linear Modulus (2)	Significance between (1)-(2) (p-value)
Radial Tension	Inner	Slow	Medium	<0.001*
			Fast	<0.001*
		Medium	Slow	<0.001*
			Fast	<0.001*
		Fast	Slow	<0.001*
			Medium	<0.001*
	Outer	Slow	Medium	<0.001*
			Fast	<0.001*
		Medium	Slow	<0.001*
			Fast	<0.001*
		Fast	Slow	<0.001*
			Medium	<0.001*
Circumferential Shear	Inner	Slow	Medium	<0.001*
			Fast	<0.001*
		Medium	Slow	<0.001*
			Fast	<0.001*

ENGR9700 - Thesis

		Fast	Slow	<0.001*
			Medium	<0.001*
	Outer	Slow	Medium	<0.001*
			Fast	<0.001*
		Medium	Slow	<0.001*
			Fast	<0.001*
	Fast	Slow	<0.001*	
		Medium	<0.001*	

4.2.3. Hysteresis Loss Ratio

The hysteresis loss ratio within each disc region for both radial tension and circumferential shear, grouped by strain rate (Figure 25).

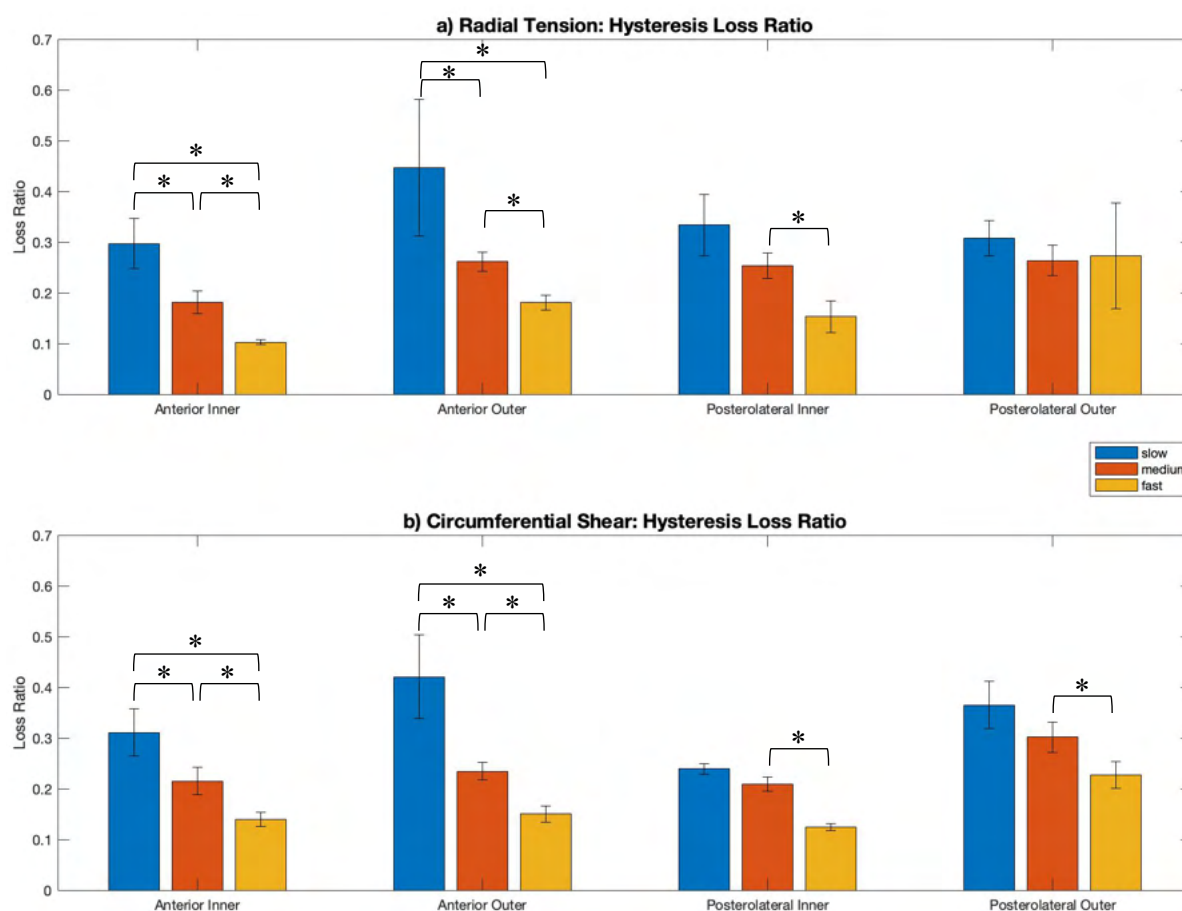


Figure 25: Hysteresis loss ratio mean with standard error bars for slow, medium and fast strain rates grouped by disc region for a) radial tension and b) circumferential shear loading directions. (* indicates statistically significant difference between results).

The overall effect of strain rate (slow, medium, fast) on the hysteresis loss ratio result was significant ($p < 0.001$). From the further interactions between strain rate and the other tested variables, a significant effect ($p = 0.044$) was also determined for the interaction between strain rate and circumferential region (Table 4). Due to the data being not normally distributed, as determined by Mauchly’s test of sphericity, the Greenhouse-Geisser method was used to assess the repeated measures ANOVA results. Hysteresis loss increased as a result of a decreased strain rate, indicating greater energy absorption at slowed loading rates. Furthermore,

hysteresis loss was found to be greater in the anterior region in comparison to the posterolateral region of the disc.

Table 4: Summary of ANOVA results for the overall effect, on hysteresis loss, of strain rate (slow, medium and fast), and the interactions between strain rate with radial region (outer and inner), circumferential region (anterior and posterolateral) and loading direction (radial tension and circumferential shear). Red and * symbol denoting statistical significance as defined by chosen alpha value (0.05), and yellow representing marginal significance ($0.05 < p < 0.1$).

Statistical Significance of Variable Effects on Hysteresis Loss Ratio	
Interaction	Significance (p-value)
Strain Rate	<0.001*
Strain Rate * Radial Region	0.599
Strain Rate * Circumferential Region	0.044
Strain Rate * Loading Direction	0.874
Strain Rate * Radial Region * Circumferential Region	0.244
Strain Rate * Radial Region * Loading Direction	0.490
Strain Rate * Circumferential Region * Loading Direction	0.869
Strain Rate * Radial Region * Circumferential Region * Loading Direction	0.657

A Bonferroni post-hoc analysis determined that there is a significant effect of strain rate between the majority of tests grouped by radial region and loading direction, irrespective of circumferential region (Table 5). The radial region and loading directions are not considered in this post-hoc comparison due to providing no overall significant effects on hysteresis loss ratio.

Table 5: Bonferroni post-hoc comparison of hysteresis loss results at slow, medium and fast strain rates, grouped by loading direction and radial region. Red and * symbol denoting statistical significance as defined by chosen alpha value (0.05), and yellow representing marginal significance ($0.05 < p < 0.1$).

Bonferroni Post-hoc Analysis of Hysteresis Loss Ratio Comparisons			
Circumferential Region	Linear Modulus (1)	Linear Modulus (2)	Significance between (1)-(2) (p-value)
Anterior	Slow	Medium	<0.001*
		Fast	<0.001*
	Medium	Slow	<0.001*
		Fast	0.001*
	Fast	Slow	<0.001*
		Medium	0.001*
Posterolateral	Slow	Medium	0.235
		Fast	0.006*
	Medium	Slow	0.235
		Fast	0.013*
	Fast	Slow	0.006*
		Medium	0.013*

4.2.4. Ultimate Stress and Strain

The ultimate stress, and corresponding strain, within each disc region for both radial tension and circumferential shear was measured (Figure 26), with a post-hoc comparison to provide assessment of the effects between subject factors.

ENGR9700 - Thesis

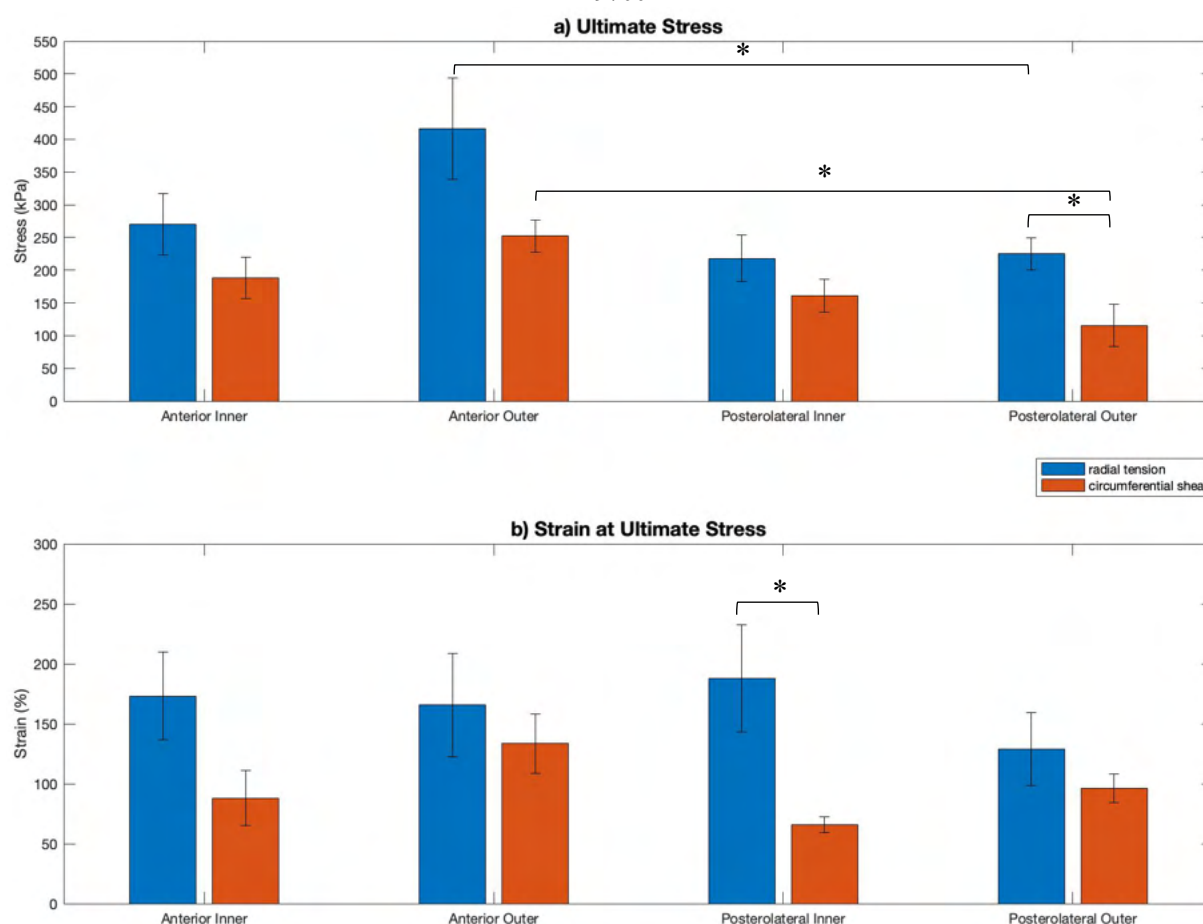


Figure 26: a) Ultimate stress and b) corresponding strain mean with standard error bars grouped based on disc region for both radial tension and circumferential shear. (* indicates statistically significant difference between results).

The overall effect of radial region was not significant ($p=0.148$) on the ultimate stress of the ILM, while the overall effect of circumferential region and loading direction were significant ($p=0.001$, mutually). The ultimate stress in the anterior region was greater than the posterolateral region. Furthermore, the ultimate stress was greater under radial tension in comparison to circumferential shear. The interaction between radial and circumferential region was also found to be significant ($p=0.039$) with a greater ultimate stress in the outer and anterior regions in comparison to inner and posterolateral regions. The effect of each of the corresponding interactions were also investigated and found to be insignificant (Table 6).

Table 6: Summary of results for the overall effect, on ultimate stress, of radial region (outer and inner), circumferential region (anterior and posterolateral) and loading direction (radial tension and circumferential shear), and the interactions between each effect. Red and * symbol denoting statistical significance as defined by chosen alpha value (0.05), and yellow representing marginal significance ($0.05 < p < 0.1$).

Statistical Significance of Variable Effects on Ultimate Stress	
Interaction	Significance (p-value)
Radial Region	0.148
Circumferential Region	0.001*
Loading Direction	0.001*
Radial Region * Circumferential Region	0.039*
Radial Region * Loading Direction	0.256
Circumferential Region * Loading Direction	0.494
Radial Region * Circumferential Region * Loading Direction	0.801

The specific regions under which the effect of loading direction on ultimate stress was significant was also determined (Table 7), with significant effects ($p=0.027$) in the posterolateral outer region and marginally significant ($p=0.078$) effects in the anterior outer region.

Table 7: Effect of loading direction on ultimate stress. Red and * symbol denoting statistical significance as defined by chosen alpha value (0.05), and yellow representing marginal significance ($0.05 < p < 0.1$).

Effect of Loading Direction on Ultimate Stress in Specific Radial and Circumferential Regions	
Disc Region	Effect Significance (p-value)
Anterior Inner	0.184
Anterior Outer	0.078
Posterolateral Inner	0.230
Posterolateral Outer	0.027*

The specific loading directions and radial regions under which the effect of circumferential region on ultimate stress was significant was also determined (Table 8), with significance effects in the outer region under both radial tension ($p=0.047$) and circumferential shear ($p=0.010$).

Table 8: Effect of circumferential location on ultimate stress within each radial region and for each loading direction. Red and * symbol denoting statistical significance as defined by chosen alpha value (0.05), and yellow representing marginal significance ($0.05 < p < 0.1$).

Effect of Circumferential Region on Ultimate Stress in Specific Radial Regions and Loading Directions		
Loading Direction	Radial Location	Effect Significance (p-value)
Radial Tension	Inner	0.402
	Outer	0.047*
Circumferential Shear	Inner	0.528
	Outer	0.010*

The overall effect of radial region and circumferential region were not significant ($p=0.918$, $p=0.353$, respectively) on the ultimate strain of the ILM, while the overall effect of loading direction was significant ($p=0.003$). The ultimate strain was greater under radial tension in comparison to circumferential shear. Each of the individual interactions between radial region, circumferential region and loading direction were found to be not significant (Table 9).

Table 9: Summary of results for the overall effect, on ultimate strain, of radial region (outer and inner), circumferential region (anterior and posterolateral) and loading direction (radial tension and circumferential shear), and the interactions between each effect. Red and * symbol denoting statistical significance as defined by chosen alpha value (0.05), and yellow representing marginal significance ($0.05 < p < 0.1$).

Statistical Significance of Variable Effects on Ultimate Strain	
Interaction	Significance (p-value)
Radial Region	0.918
Circumferential Region	0.353
Loading Direction	0.003
Radial Region * Circumferential Region	0.446
Radial Region * Loading Direction	0.108
Circumferential Region * Loading Direction	0.668
Radial Region * Circumferential Region * Loading Direction	0.675

The specific regions under which the effect of loading direction on ultimate strain was significant was also determined (Table 10), with significant effects ($p=0.027$) in the

posterolateral inner region and marginally significant ($p=0.085$) effects in the anterior inner region.

Table 10: Effect of loading direction on ultimate strain. Red and * symbol denoting statistical significance as defined by chosen alpha value (0.05), and yellow representing marginal significance ($0.05 < p < 0.1$).

Effect of Loading Direction on Ultimate Strain in Specific Radial and Circumferential Regions	
Disc Region	Effect Significance (p-value)
Anterior Inner	0.085
Anterior Outer	0.536
Posterolateral Inner	0.027*
Posterolateral Outer	0.346

5. Discussion

5.1. Results Interpretation

Understanding the specific mechanical properties of the human ILM and the dependence on factors such as radial (inner vs. outer) and circumferential (anterior vs. posterolateral) disc region, loading direction and strain rate allow for a more comprehensive knowledge of the AF and disc mechanics as whole, complex structures. This study is the first within the field to directly assess the human ILM behaviour, providing innovative insights with a particular focus on regional variation. Overall, the ILM demonstrated greater strength and modulus in outer and anterior regions of the disc. With these regional differences attributed to varied mechanics between the region of the disc.

5.1.1. Toe Modulus

The overall effect of loading direction on the toe modulus was not significant ($p=0.867$), with no identifiable trends apparent. This indicates that the amount of stretching out, or fibre reorganisation that the ILM is undergoing before entering the linear stage is not dependent on whether it is being loaded in the radial tension or circumferential shear direction. The variation in elastic fibre orientation of the ILM (Yu, et al. 2002) (Tavakoli, et al. 2016) would justify an expectation for the length of the toe modulus to be greater under radial tension in comparison to circumferential shear in the outer regions of the disc. The elastic fibre orientation parallel to the collagen fibre network of lamellae in the outer ILM would lead to greater strain required to result in fibre recruitment in the radial direction in comparison to the shear direction. However, it was not possible to determine this trend from the results. However, the interaction effect of strain rate with radial region and loading direction was marginally significant ($p=0.07$), indicating the presence of this trend when paired with radial region effects.

The overall effect of strain rate on the toe modulus was significant ($p=0.002$), with the no further interactions identifying significance in any of the disc regions. The results demonstrate that at a faster strain rate, the toe modulus is greater. This is strongly indicative of the

viscoelastic properties of the ILM, as identified by the strain-rate dependent stress response of soft tissue (Sengul, 2021) (Sanjeevi, 1982). The lack of significant difference in the further interaction tests may be due to this study's specimen specific toe region identification. Due to machine preload variation, the 100mN target was not consistently reached prior to each test, leading to variability in toe region behaviour between specimens. Therefore, there is a degree of subjectivity when visually identifying the toe region for each test, leading to possible variances between specimens. Regardless, the significant effect of strain rate on the toe modulus results was still identified, confirming the viscoelastic response of the ILM.

Radial and circumferential regional variation were also found to have effects with non-significance. Although this is so, a visible radial trend can be seen (Figure 23) for the specimens undergoing radial tension, with the outer regions displaying an observably greater toe modulus than the corresponding inner regions. This trend is not apparent in the specimens under circumferential shear. Under radial tension, the toe modulus within the outer anterior region was greater than the outer posterolateral region, while minimal disparity is observed in the inner regions. This trend being apparent exclusively in the outer region may be attributed to the more homogeneous fibre orientation in comparison to the inner regions, also indicating a more uniform fibre recruitment in the early stages of loading. Under circumferential shear, there are no identifiable trends between the specific regions, requiring further work to verify any trends that may have been unapparent.

5.1.2. Linear Modulus

The linear modulus of a material represents the material's resistance to the load that is being applied. For the context of the human ILM, this modulus represents the resistive forces of the adjacent lamellae to being separated radially (tension) and circumferentially (shear). This is integral to the mechanical performance of the disc, with the ILM representing the boundaries between lamellae where failure can initiate and lead to tearing and herniation.

Although loading direction was not found to have a significant effect on the linear modulus, the overall trend demonstrates that the linear modulus of the ILM is greater under circumferential shear in comparison to radial tension, particularly in the inner AF (Figure 24). The linear modulus being greater under circumferential shear is contradictory to findings established on ovine specimens (Tavakoli & Costi, 2018), indicating a significant distinction between the mechanical properties of human and ovine ILM under various loading directions. This remarkable finding requires a detailed assessment of the microstructure of the ILM elastic fibre network, which has yet to be undertaken. Studies comparing the tensile modulus of the lamellae from various species (Monaco, et al. 2015) indicated that the ovine lamellae tensile modulus (0.87MPa) is greater than previously investigated human results (0.22MPa). The

increased modulus of ovine discs in comparison to human discs appears to be apparent in the ILM in addition to the lamellae. The average linear modulus of the ILM found during this study under radial tension and circumferential shear, across all strain rates and regions, was approximately 0.23MPa and 0.50MPa, respectively. While previously found corresponding values for ovine elastic fibre mechanical properties of the ILM were approximately 1.3MPa and 0.9MPa, respectively (Tavakoli & Costi, 2018). Comparatively, this discrepancy between human and ovine specimens indicates that the human ILM demonstrates a lesser linear modulus than that of the ovine tissue and also indicates that the greater modulus is in the contradictory loading direction between species, being greater in tension for ovine and greater in shear for human. This inconsistency between sheep and human may be attributed to the age of the specimens used for each study. The average human donor age of 56 in comparison to the young ovine specimens used (18-24 months), impacts the tissue composition of the disc (Colombini, et al. 2008) (Hardingham & Fosang, 1992) and subsequently the mechanical performance.

The overall effect of strain rate on the linear modulus resulted in trends that were significantly different ($p < 0.001$), with all of the specific test comparisons demonstrating a statistically significant effect of strain rate. A strong trend is apparent that the modulus is greater at a faster strain rate in comparison to slower strain rates for all disc regions in both loading directions. This is an indication of the viscoelastic properties of the human ILM tissue as expected based on previous studies (Tavakoli & Costi, 2018). In a viscoelastic material, fluid flow plays an integral role in the mechanical performance of the material. As a load is applied to the human tissue, the volume is altered causing water flow within the tissue. At a slower strain rate, the increased loading time period allows for more water loss from the loaded tissue, with the solid components of the tissue providing the majority of the mechanical integrity. At a greater strain rate, the water is unable to flow through the permeable matrix of fibres and cells, creating large frictional drag forces, allowing for the fluid phase of the tissue to provide significant mechanical properties, increasing stiffness and hence, modulus. This behaviour of the tissue is referred to as the biphasic viscoelastic phenomenon (Ehlers & Markert, 2001). Under pure shear loading conditions, there is geometric changes with no volume change, resulting in no fluid flow within the tissue. Due to this, the stiffness would still increase with an increased strain rate but to a lesser degree in comparison to under radial tension. Although the limitations of this study to provide 100% pure shear will inhibit the ability of the results to demonstrate this, the phenomena is still apparent in the results of this study with the average difference in modulus between slow and fast strain rates for tension and shear being 54% and 34% respectively. Therefore, this limitation was inhibited and the results

still valid in representing the effect of strain rate in both radial tension and circumferential shear.

Although radial and circumferential region within the disc displayed non-significant effects on the linear modulus of the ILM, some overall trends can still be identified with the outer AF having a greater modulus in radial tension than the inner AF. The significant effect of the interaction between strain rate, radial region and loading direction ($p=0.014$), supports this observable trend. This is expected due to the increased level of fibre organisation of the ILM in the outer AF in comparison to the less structured inner AF and transitional region closer to the nucleus. The elastic fibres of the outer AF have been found to be aligned parallel to the lamellae when unloaded and become recruited under radial tension, providing resistance to tension between adjacent lamellae (Smith & Fazzalari, 2006). Conversely, the elastic fibre orientation within the inner AF have a less homogeneous arrangement, resulting in less specific recruitment of the fibres under radial tension. The density of elastic fibres in the ILM is also greater in the outer regions in comparison to the inner AF (Tavakoli, et al. 2017), providing increased mechanical integrity as supported by the greater modulus found in this study. This trend is not apparent when the ILM is loaded in the circumferential shear direction, indicating that the mechanical performance of the ILM during cyclic loading in the circumferential shear direction is less dependent on disc region in comparison to radial tension and requires further investigation.

5.1.3. Hysteresis Loss

The hysteresis loss ratio is representative of the amount of energy lost during the loading cycle, normalised by the amount of energy applied. A greater hysteresis loss ratio indicates greater energy loss while a reduced loss ratio indicates that the ILM is behaving closer to that of an elastic material, where the energy is stored during loading and equally released when unloaded.

Loading direction provided no significant effect on the hysteresis loss ratio of the ILM, indicating that the energy lost during loading is independent of whether the specimens were loaded under radial tension or circumferential shear. This is contradictory to previous comparable studies (Tavakoli & Costi, 2018) indicating an increased phase angle under circumferential shear in comparison to radial tension in ovine specimens. Phase angle is an alternate parameter than can be calculated in order to determine the energy loss under cyclic loading, and therefore the results from Tavakoli's study indicate that an increased hysteresis loss ratio would be expected under circumferential shear. Although the results from this study do not indicate this, further investigation will be required in order to make any confirmations. This inconsistency between human and ovine may indicate that a greater strain than 40% is

required to be applied to human ILM to observe the same trends, being more extensible than ovine ILM.

The strain rate had a significant ($p < 0.001$) effect on the results of the hysteresis loss ratio, with a slower strain rate resulting in increased hysteresis loss. This is indicative that the amount of energy lost during loading is greater if the load is applied at a slower rate. Intuitively, this would be due to the increased water flow from the tissue at a slower strain rate, resulting in the energy dissipating as the water flows out of the ILM tissue. At greater strain rates, less water flows from the ILM, and the tissue behaves similarly to a non-linear elastic material, with minimal energy loss (approximately 17% compared to 34% at a slow strain rate). Being loaded at a slower strain rate allows more time for the tissue to demonstrate stress relaxation behaviour during the cycle, reducing the elasticity of the ILM.

The interaction between strain rate and circumferential region was found to produce significant effects ($p = 0.044$) on the hysteresis loss ratio with specimens from the anterior region having a greater hysteresis loss than the posterolateral. Supporting this finding, a greater elastic fibre density in the posterolateral AF (Tavakoli, et al. 2016) would be expected to result in less hysteresis loss in posterolateral regions relative to anterior AF. Greater elastic fibre density, tissue organisation and lower water volume would be expected to result in less water flow from the tissue under loading conditions, resulting in less energy loss.

5.1.4. *Ultimate Stress and Strain*

The ultimate stress of the ILM occurs after the yield point has been surpassed for the specimen, meaning that deformation has occurred, and the tissue cannot return to its original configuration. The measured ultimate stress provides a greater understanding of the overall strength of the ILM and the strain at which this ultimate stress occurs is indicative of how much strain the specimen can endure prior to failure.

Significant overall effect of loading direction on ultimate stress ($p = 0.001$) and the corresponding strain ($p = 0.003$) was observed. Both the ultimate stress and the corresponding strain in the radial tension loading direction were significantly greater than that under circumferential shear. This greater ultimate stress indicates that the ILM can endure a greater load in the radial tension direction in comparison to the shearing direction, providing greater mechanical strength to disc in the radial direction. Therefore, a greater stress is required to cause delamination in the AF if the load is applied radially rather than circumferentially, consistent with previous studies on ovine ILM (Tavakoli & Costi, 2018). This increased strength in the ILM in tension could be attributed to the presence of trans-lamellar cross-bridges, with the only known source of collagen fibres in the ILM (Tavakoli, et al. 2016) providing increased mechanical integrity under tension. The greater strain in order to reach

ultimate stress under radial tension in comparison to shear indicates that a greater strain is required for full fibre recruitment in tension. This is consistent with literature indicating the orientation of the elastic fibres in the ILM being parallel to the lamella when unloaded (Tavakoli, et al. 2017). Once radial tension is applied, the fibres must re-orientate perpendicularly before full recruitment, increasing the maximum strain before failure. Conversely, when circumferential shear is applied, the fibres are already oriented parallel to the loading direction, reducing the amount of strain required for full fibre recruitment. However, this result does not agree with previously found data on ovine specimens (Tavakoli & Costi, 2018), indicating that the failure strain is greater for shear in comparison to tension.

Although the overall effect of radial region was found to be non-significant ($p=0.148$ and $p=0.918$, respectively) on the ultimate stress and the corresponding strain, indications of potential trends can be identified. The overall effect of circumferential region ($p=0.001$) and the interaction between radial and circumferential region ($p=0.039$) were significant on the ultimate stress. Under radial tension and circumferential shear, the outer anterior region demonstrated an observably greater ultimate stress than the inner region, in agreement with previous findings on the delamination strength being greater in the outer AF (Gregory, et al. 2011). Under both tension and shear loading, the outer anterior region demonstrated significantly ($p=0.047$ and $p=0.010$, respectively) greater ultimate stress values than the outer posterolateral region, consistent with literature validating that the AF in the posterolateral region contains a greater percentage of incomplete lamellae with a looser connection between lamellae (Tsuji, et al. 1993). The decreased strength in the posterolateral region is indicative of the evidence supporting the increased relative prevalence of herniation and failure occurring in the posterolateral region of the disc (Wathen, et al. 2018) (Donegan & Chin, 2009). The strain corresponding to the ultimate stress was found to be greater in the outer regions in comparison to the inner AF and greater in the anterior region in comparison to the posterolateral region, particularly under shear loading. This indicates that less strain is required, in shear, to result in ILM failure for the inner and posterolateral AF, further supporting the prevalence of failure in the posterolateral and inner regions of the disc.

5.2. *Limitations of Study*

There are a number of limitations impacting the overall results of this study that must be considered when analysing the significance of the results. The first and most prevalent of these limitations is the use of the minimal acceptable sample size to allow for significant results. Due to limited availability of specimens, the sample size used was calculated as the minimum possible in order to detect a large effect size for this test setup. In order to identify smaller effect sizes of each independent variable to a significant degree, a larger sample size would be

required. For example, a sample size of $N=11$ would be required to detect a medium effect as outlined by Cohen's Criteria, and a sample size of $N=58$ to detect a small effect (G*Power Version 3.1.9.6, Heinrich Heine University, Dusseldorf). Although this study may be indicative of specific trends, a larger sample size would be required in order to validate the significance of these trends.

Another considerable limitation of this study is the ability to provide an accurate measure of the cross-sectional area of the specimen during testing. As deformation occurs throughout the loading period, the cross-sectional area of the region of interest alters. The stress is calculated using the initial cross-sectional area rather than being able to measure the instantaneous cross-sectional area for more accurate stress calculations. This will provide systematic error to the results and will result in an underestimation of the true stresses experienced by the ILM.

The ability to provide pure shear strain to the ILM is also limited by the experimental setup of this study. Due to the geometry of the disc, the ILM boundary is arc-shaped rather than linear, limiting the ability to provide pure shear with linear actuators. This limitation was mitigated by reducing the width of the specimens for shear testing, reducing the arc angle of the ILM boundary and minimising the relative curvature. Regardless of this, the boundary is still intrinsically curved, inhibiting the ability for pure shear to be applied.

For this study, the outer AF region was found by identifying a lamellae-ILM-lamellae junction within 1-5 lamellae from the superficial layer that is also visibly complete and appears structurally undamaged. The same procedure was followed for the inner regions between 10-15 lamellae. This resulted in an ILM of inconsistent depth to be isolated for testing within the 'outer' region group and within the 'inner' region group. With the smaller sample size, this regional variation would not be significant enough to directly affect the results but should be considered for larger sample size studies.

6. Conclusions

The aim of this study was to increase the depth of knowledge into the field of human ILM mechanical properties. For the first time, this study provides the a comprehensive assessment of the regional variation in human ILM mechanical performance, with a focus on the inner and outer AF regions. This was done by conducting uniaxial tensile loading to isolated human lumbar ILM specimens from anterior and posterolateral regions within the disc in two different loading directions at three defined strain rates.

Radial (outer vs. inner) and circumferential (anterior vs. posterolateral) regional variation trends were identified in the modulus, ultimate stress and strain results but at a limited

significance, suspectedly due to the limited sample size. It was identified that the modulus was greater in the outer and anterior disc regions in comparison to the inner and posterolateral regions, respectively. Furthermore, the ultimate stress was greater in the outer regions compared to the inner under radial tension and the anterior specimens demonstrated a greater ultimate stress than posterolateral specimens, particularly in the outer AF. The stress at which ultimate strain occurs was also greater in the outer AF under circumferential shear loading.

As hypothesised, the modulus and hysteresis loss during loading was significantly impacted by the strain rate, with strong viscoelastic behaviour indicated by a greater modulus as a result of an increased strain rate. The energy lost under cyclic loading, indicated by hysteresis loss ratio was reduced as strain rate is increased, behaving more similarly to a non-linear elastic material.

The loading direction also had a significant impact on the linear modulus, the ultimate stress and strain with loading in circumferential shear providing a significantly greater modulus in comparison to radial tension. Both the ultimate stress and the strain at which this stress was reached were significantly greater under radial tension in comparison to circumferential shear, indicating greater strength and extensibility.

This research provides a number of novel insights in the context of a valuable preliminary study that has the potential to be expanded upon more thoroughly for further validation.

7. Future Work

The work done throughout this study provides sound methodologies and a base knowledge with the potential to expand upon and further increase the understanding of the human lumbar ILM mechanical properties. Through increased funding and support, a more expansive study should be conducted with a considerably greater sample size in order to identify and validate any effects of smaller size. A study such as this may include a more extensive analysis of the disc region variation by collecting specimens from various circumferential locations throughout the disc including lateral and anterolateral in addition to the anterior and posterolateral investigated in this study. A more systematic approach should also be applied in order to increase the consistency in ‘outer’ and ‘inner’ region identification between specimens. Investigations into the mechanical contribution of the various components to the structural integrity of the ILM should also be considered. This could be analysed by using methods of enzymatic digestion to isolate various components before mechanical testing and comparing the results to the intact ILM performance. Although similar studies have been conducted in other species (Tavakoli, 2018), there have not been any published efforts to apply this methodology to human specimens. There has also been previous work done to assess the

mechanical properties of the human AF under more anatomically representative biaxial loading conditions (Gregory & Callaghan, 2011), a similar approach applied to the human ILM would provide great insights into the mechanical behaviour during in-vivo loading. A comprehensive assessment of the variation across lumbar levels, in addition to the L1-L2 investigated in this study, would also provide further, valuable insights. Furthermore, the effects of disc degeneration and injury, in conjunction with tissue engineering repair strategies would provide an invaluable contribution to the field.

Although considerable work has been done to deepen the knowledge of the human ILM structure and mechanical properties, the unknowns still greatly outweigh confirmed knowledge. There are various areas of research within this field that can, and should, be focused on for further investigation in the coming years to improve the accuracy of computational modelling and anatomical implant design for subsequent generations.

8. References

- Bogduk, N. Clinical anatomy of the lumbar spine and sacrum, (3rd ed.) Churchill Livingstone, New York, 1997.
- Bruehlmann, SB, Rattner, JB, Matyas, JR & Duncan, NA 2002, 'Regional variations in the cellular matrix of the annulus fibrosus of the intervertebral disc', *Journal of Anatomy*, vol. 201, pp. 159-171.
- Buckwalter, JA 1995, 'Aging and degeneration of the human intervertebral disc', *Spine*, vol. 20, no. 11, pp. 1307-1314.
- Cassidy, JJ, Hiltner, A & Baer, E 1989, 'Hierarchical structure of the intervertebral disc', *Connective Tissue Research*, vol. 23, pp. 75-88.
- Castro, APG & Lacroix, D 2017, Computational modelling of the intervertebral disc: A case study for biomedical composites, Biomedical Composites (second edition), Woodhead Publishing Series in Biomaterials, pp. 479-500.
- Colombini, A, Lombardi, G, Corsi, MM & Banfi, G 2008, 'Pathophysiology of human intervertebral disc', *The International Journal of Biochemistry & Cell Biology*, vol. 40, no. 5, pp. 837-842.
- Donegan, DJ & Chin, KR 2009, *Gowned and gloved orthopaedics: Introduction to common procedures: Lumbar microdiscectomy*.
- Ehlers, W & Markert, B 2001, 'A linear viscoelastic biphasic model for soft tissues based on the Theory of Porous Media', *Journal of Biomechanical Engineering*, vol. 123, no. 5, pp. 418-424.
- Gregory, DE, Bae, WC, Sah, RL & Masuda, K 2011, 'Annular delamination strength of human lumbar intervertebral disc', *European Spine Journal*, vol. 21, pp. 1716-1723.
- Gregory, DE & Callaghan, JP 2011, 'A comparison of uniaxial and biaxial mechanical properties of the annulus fibrosus: a porcine model', *Journal of Biomechanical Engineering*, vol. 133, no. 2, pp. 024503/1-024503/5.
- Gregory, DE & Callaghan, JP 2012, 'An examination of the mechanical properties of the annulus fibrosus: The effect of vibration on the intralaminar matrix strength', *Medical Engineering and Physics*, vol. 34, pp. 472-477.
- Gruber, HE & Hanley Jr. EN 2002, 'Observation on the morphological changes in the aging and degenerating human disc: Secondary collagen alterations', *BMC Musculoskeletal Disorders*, vol. 3, no. 9, pp. 1-6.
- Hardingham, TE & Fosang, JA 1992 'Proteoglycans: many forms and many functions', *Federation of American Societies for Experimental Biology*, vol. 6, no. 3, pp. 861-870.
- Harvey-Burgess, M & Gregory, DE 2019, 'The effect of axial torsion on the mechanical properties of the annulus fibrosus', *Spine*, vol. 44, no. 4, pp. E195-E201.
- Holzappel, GA, Shulze-Bauer, CAJ, Feigle, G & Regitnig, P 2005, 'Single lamellar mechanics of the human lumbar annulus fibrosus', *Biomechanics and Modelling in Mechanobiology*, vol. 3, pp. 125-140.
- Humzah, MD, Soames, RW 1988, 'Human intervertebral disc: Structure and function', *The Anatomical Record*, vol. 288, pp. 337-356.
- Iatridis, JC & Gwynn, I 2004, 'Mechanisms for mechanical damage in the intervertebral disc annulus fibrosus', *Journal of Biomechanics*, vol. 37, pp. 1165-1175.
- Inoue, H & Takeda, T 2009, 'Three-dimensional observation of collagen framework of lumbar intervertebral discs', *Acta Orthopaedica Scandinavica*, vol. 46, no. 6, pp. 949-956.
- Marchand, F & Ahmed, AM 1990, 'Investigation of the laminate structure of lumbar disc annulus fibrosus', *Spine*, vol. 15, no. 5, pp. 402-410.
- Marcolongo, M, Sarkar, S & Ganesh, M 2017, *Comprehensive biomaterials: Trends in materials for spine surgery*, vol. 7, Drexel University, Philadelphia, USA.
- Martin, NC, Pirie, AA, Ford, LV, Callaghan, CL, McTurk, K, Lucy, D & Scrimger, DG 2006, 'The use of phosphate buffered saline for the recovery of cells and spermatozoa from swabs', *Science & Justice*, vol. 46, no. 3, pp. 179-184.
- Nachemson, A & Morris, JM 1964, 'In vivo measurements of intradiscal pressure: Discometry, a method for the determination of pressure in the lower lumbar discs', *The Journal of Bone & Joint Surgery*, vol. 46, no. 5, pp. 1077-1092.
- Newell, N, Little, JP, Christou, A, Adams, MA, Adam, CJ & Masouros, SD 2017, 'Biomechanics of the human intervertebral disc: A review of testing techniques and results', *Journal of the Mechanical Behavior of Biomedical Materials*, vol. 69, pp. 420-434.
- Noailly, J, Planell, JA & Lacroix, D 2010, 'On the collagen criss-cross angles in the annuli fibrosi of lumbar spine finite element models', *Biomechanics and Modelling in Mechanobiology*, vol. 10, pp. 203-219.
- Pezowicz, J 2010, 'Analysis of selected mechanical properties of intervertebral disc annulus fibrosus in macro and microscopic scale', *Journal of Theoretical and Applied Mechanics*, vol. 48, no. 4, pp. 917-932.
- Roberts, S, Evans, H, Trivedi, J and Menage, J 2006, 'Histology and pathology of the human intervertebral disc', *Journal of Bone and Joint Surgery*, vol. 88, no. 2, pp.10-14.
- Roughley, PJ 2004, 'Biology of intervertebral disc aging and degeneration: Involvement of the extracellular matrix', *The Spine Journal*, vol. 29, no. 23, pp. 2691-2699.
- Sanjeevi, R 1982, 'A viscoelastic model for the mechanical properties of biological materials', *Journal of Biomechanics*, vol. 15, no. 2, pp. 107-109.
- Schollum, ML, Robertson, PA & Broom, ND 2008, 'ISSLS prize winner: Microstructure and mechanical disruption of the lumbar disc annulus', *Spine*, vol. 33, no. 25, pp. 2702-2710.
- Schollum, ML, Robertson, PA & Broom, ND 2009, 'A microstructural investigation of intervertebral disc lamellar connectivity: detailed analysis of the translamellar bridges', *Journal of Anatomy*, vol. 214, no. 6, pp. 805-816.
- Sengul, Y 2021, 'Nonlinear viscoelasticity of strain rate type: An overview', *Proceedings of the Royal Society A: Mathematical, Physical and Engineering Sciences*, vol. 477, no. 2245.

ENGR9700 - Thesis

- Smith, LJ, Byers, S, Costi, JJ & Fazzalari, NL 2007, 'Elastic fibers enhance the mechanical integrity of the human lumbar annulus fibrosus in the radial direction', *Annals of Biomedical Engineering*, vol. 36, no. 2, pp. 214-22.
- Smith, LJ & Elliott, DM 2011, 'Formation of lamellar cross bridges in the annulus fibrosus of the intervertebral disc is a consequence of vascular regression', *Matrix Biology*, vol. 30, pp. 267-274.
- Smith, LJ & Fazzalari, NL 2006, 'Regional variations in the density and arrangement of elastic fibres in the annulus fibrosus of the human lumbar disc', *Journal of Anatomy*, vol. 209, no. 3, pp. 359-367.
- Stewart, DM, Monaco, LA & Gregory, DE 2017, 'The aging disc: using an ovine model to examine age-related differences in the biomechanical properties of the intralamellar matrix of single lamellae', *European Spine Journal*, vol. 26, pp. 259-266.
- Tavakoli, J, Elliott, DM & Costi, JJ 2016, 'Structure and mechanical function of the inter-lamellar matrix of the annulus fibrosus in the disc', *Journal of Orthopaedic Research*, vol. 34, no. 8, pp. 1307-1315.
- Tavakoli, J, Elliott, DM & Costi, JJ 2017, 'The ultra-structural organization of the elastic network in the intra- and inter- lamellar matrix of the intervertebral disc', *Acta Biomaterialia*, vol. 58, pp. 269-277.
- Tavakoli, J & Costi, JJ 2018, 'New findings confirm the viscoelastic behaviour of the inter-lamellar matrix of the disc annulus fibrosus in radial and circumferential directions of loading', *Acta Biomaterialia*, vol. 71, pp. 411-419.
- Tavakoli, J & Costi, JJ 2018, 'New insights into the viscoelastic and failure mechanical properties of the elastic fiber network of the inter-lamellar matrix in the annulus fibrosus of the disc', *Acta Biomaterialia*, vol. 77, pp. 292-300.
- Tsuji, H, Hirano, N, Ohshima, H, Ishihara, H, Terahata, N & Motoe, T 1993, 'Structural variation of the anterior and posterior annulus fibrosus in the development of human lumbar intervertebral disc. A risk factor for intervertebral disc rupture', *Spine*, vol. 18, no. 2, pp. 204-210.
- Wathen, C, Mullin, JP, Chan, AY & Benzel, EC 2018, *Principles of neurological surgery: Degenerative spinal disease (lumbar)*, 4th edition, Elsevier.
- Yu, J 2002, 'Elastic tissues of the intervertebral disc', *Biochemical Society Transactions*, vol. 30, no. 6, pp. 848-852.
- Yu, J, Winlove, PC, Roberts, S & Urban, JPG 2002, 'Elastic fibre organization in the intervertebral discs of the bovine tail', *Journal of Anatomy*, vol. 201, no. 6, pp. 465-475.

Appendix A – Detailed Donor Information and Specimen Dimensions

Information provided from the United Tissue Network (USA) was used in order to make selections of the donors to be used as subjects for this study and the relevant information of the selected subject was then compiled (Table 11). The measured dimensions of the L1-L2 disc from the selected donors was also used to approximate the disc volume (Table 12), with a parameter definition provided (Table 13).

Table 11: Donor age, sex and known relevant health information.

Donor	Date of death	Age (years)	Sex	Known health related information
D1	25/03/2016	58	Male	Known diseases/illnesses: none
D2	05/05/2019	59	Male	BMI: 22.1 Bladder cancer positive Former tobacco user (earlier in life) Physically active: yes
D3	18/03/2019	74	Male	BMI: 31.3 Non-Hodgkin's lymphoma positive Former tobacco user (earlier in life) Physically active: yes Hypertension and implanted pacemaker Dementia Type II diabetes positive
D4	07/05/2019	66	Female	Cardiovascular disease Heavy smoker Physically active: yes Rheumatoid arthritis
D5	24/03/2019	25	Male	BMI: 22.1 Known diseases/illnesses: none Physically active: yes Tobacco use: yes

Table 12: Disc dimensions from each specimen, as defined in Table 21, and the approximation of cross-sectional area intact volume.

Specimen	H _A	H _L	W	D	Approximated disc area (mm ²)	Approximated volume (mm ³)
D1: L1-L2	11.1	11.5	71.2	59.8	2830.4	31983.8
D2: L1-L2	13.1	13.4	75.1	60.5	3032.7	40183.2
D3: L1-L2	8.3	10.3	77.9	54.5	2891.2	26888.7
D4: L1-L2	10.3	9.2	60.7	63.1	2527.8	24646.5
D5: L1-L2	11.1	10.5	69.7	48.6	2308.2	24928.8

Table 13: Dimensional symbol definitions of measurements taken from each specimen.

Symbol	Definition
H _A	The height of the disc from end plate to end plate as viewed from the anterior view.
H _L	The height of the disc from end plate to end plate as viewed from the lateral view.
W	The width of the disc measured as the distance between the two most lateral points from the anterior view.
D	The depth of the disc measured as the distance from the furthest point anteriorly to the furthest point posteriorly, from the lateral view.

Appendix B – Cyclic Loading and Failure Data for All Specimens

The final loading cycle for each specimen and the failure curve used for calculations can be seen in the figures from this section.

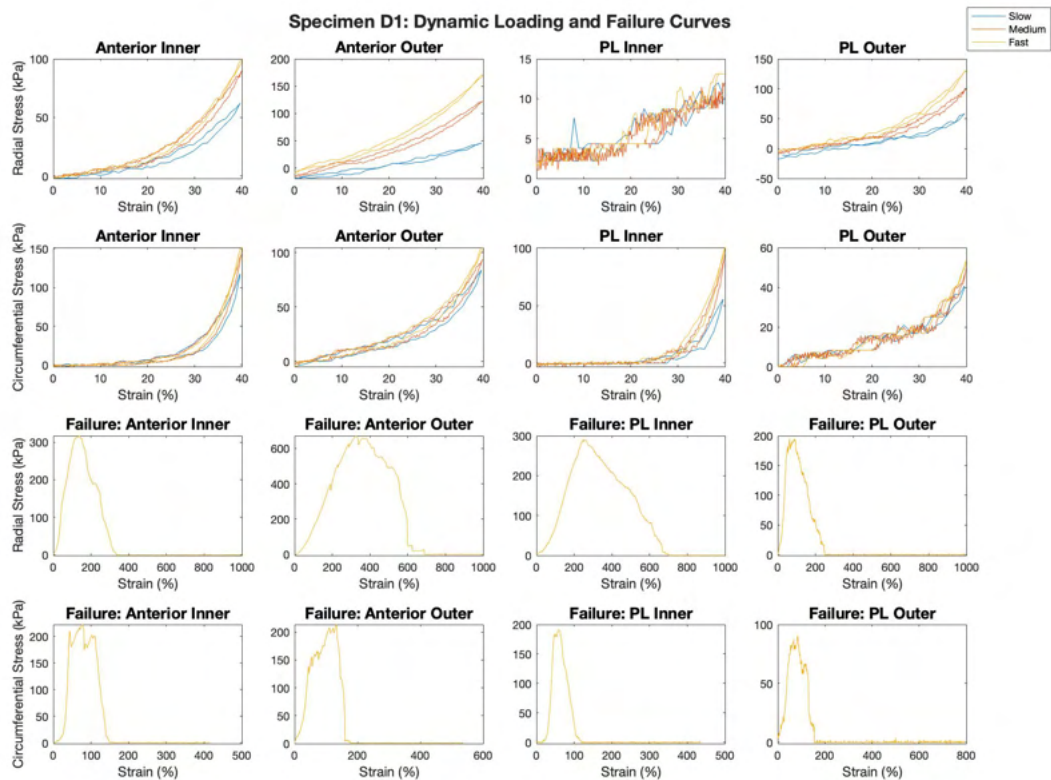


Figure 27: All analysed loading cycles for slow, medium, fast and failure tests for D1.

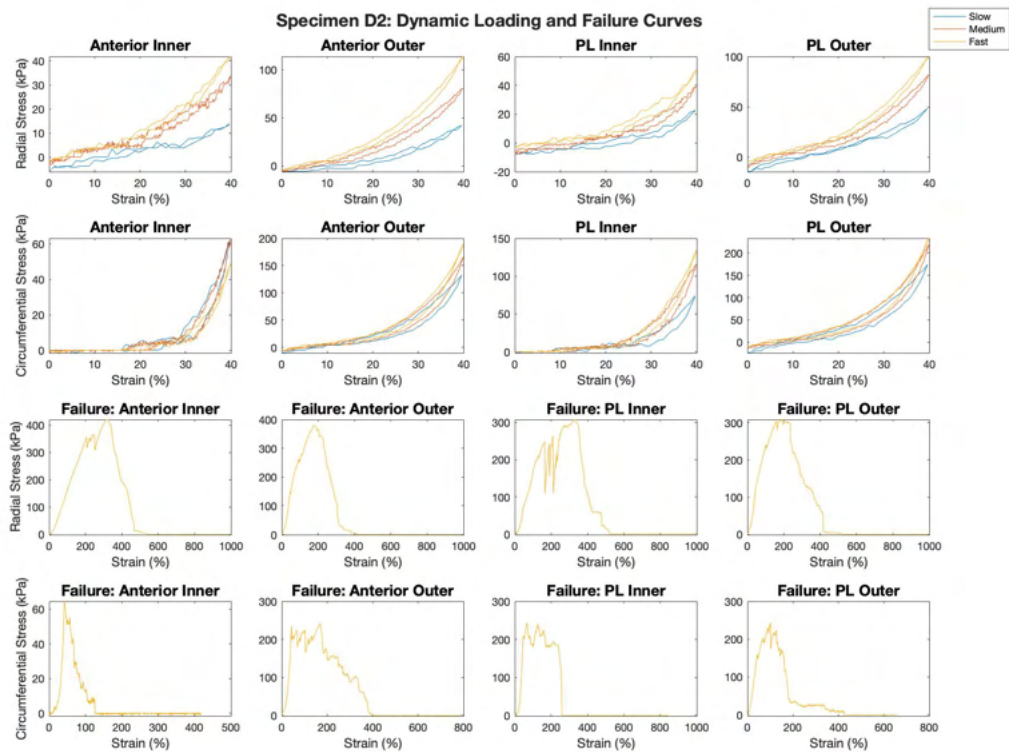


Figure 28: All analysed loading cycles for slow, medium, fast and failure tests for D2.

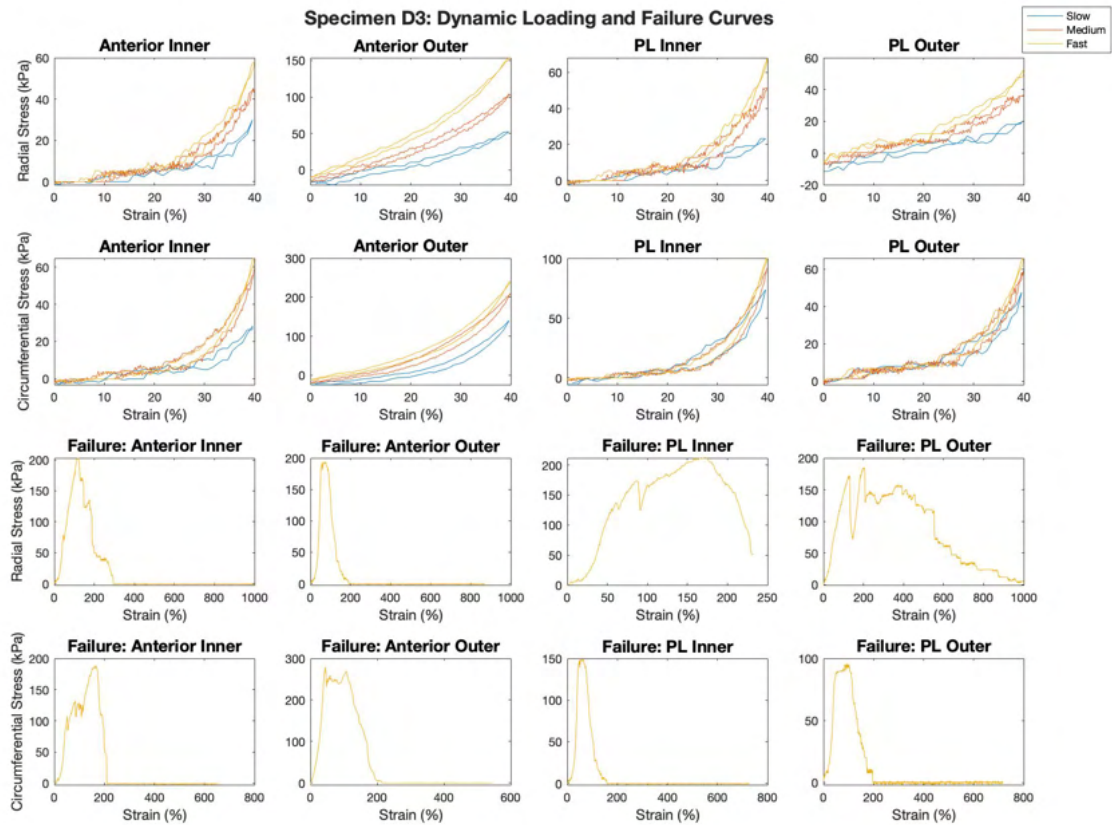


Figure 29: All analysed loading cycles for slow, medium, fast and failure tests for D3.

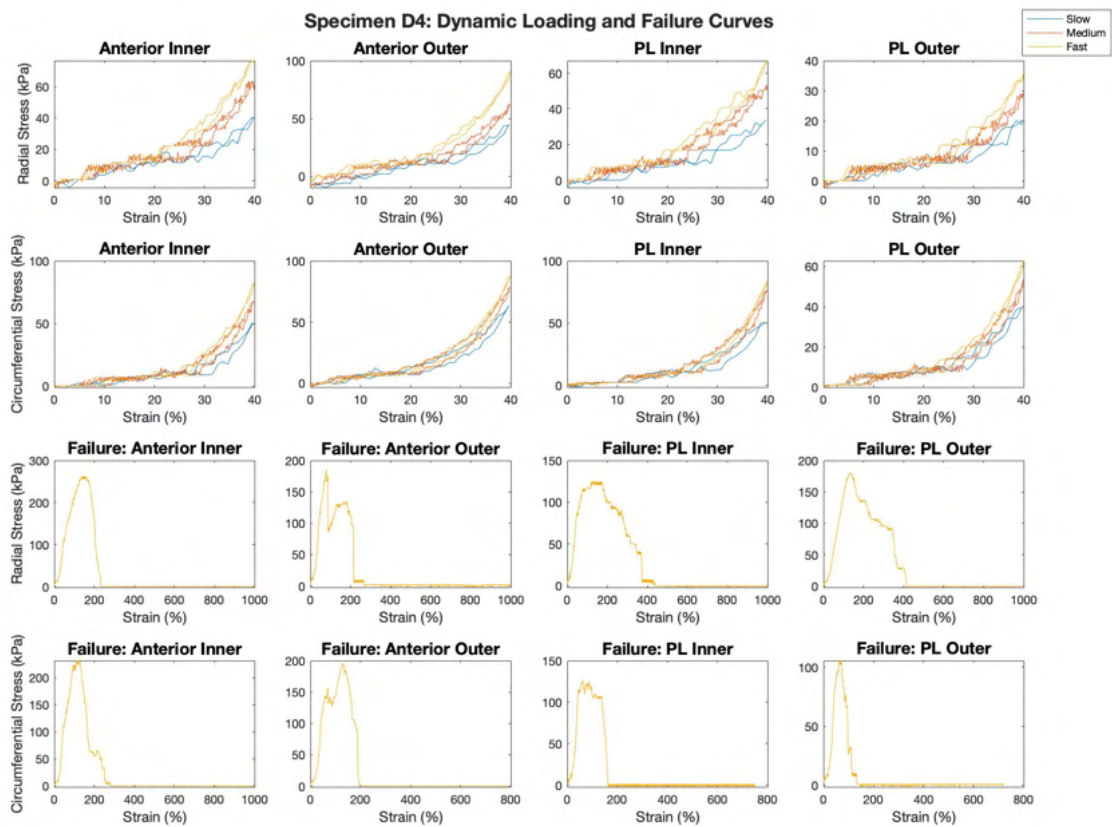


Figure 30: All analysed loading cycles for slow, medium, fast and failure tests for D4.

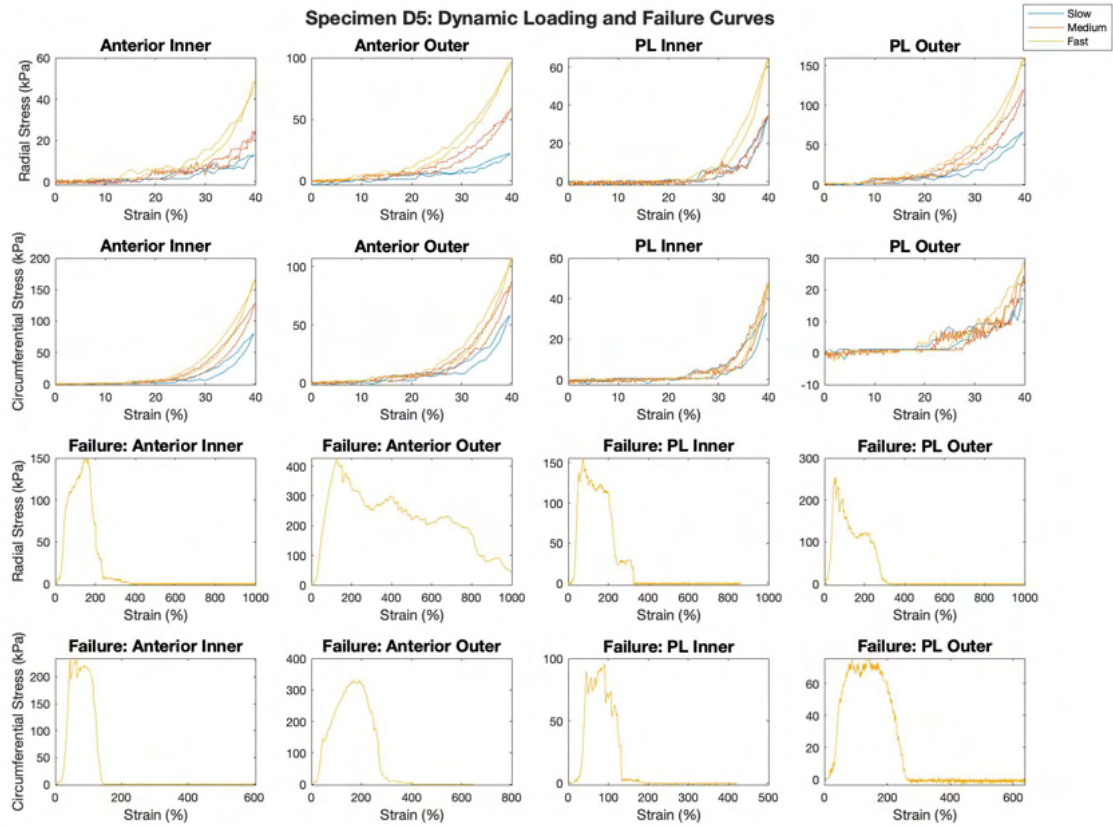


Figure 31: All analysed loading cycles for slow, medium, fast and failure tests for D5.